Hirai and Kadobayashi
Progress in Earth and Planetary Science (2023) 10:3
https://doi.org/10.1186/s40645-023-00534-6

Progress in Earth and Planetary Science

REVIEW

Open Access

Significance of the high-pressure properties and structural evolution of gas hydrates for inferring the interior of icy bodies

Hisako Hirai[1*] and Hirokazu Kadobayashi[2*]

Abstract

Hydrogen, methane, and water ice are among the most abundant materials in the universe. Based on experimental, theoretical, and spacecraft data, gas hydrates consisting of gas and water ice have been predicted to exist throughout the universe. This review discusses the high-pressure properties of two common gas hydrates (methane and hydrogen hydrates) at low and high temperatures based primarily on experimental results. Gas hydrates consist of a water molecule host and a gaseous guest. They have a clathrate structure at low pressure and a filled-ice structure at high pressure. The host encloses the guest, and a specific interaction occurs between the guest and host, resulting in unique physical properties. When subjected to pressure, gas hydrates undergo various phase changes. Based on pressure and guest size, a general rule for phase changes occurring in gas hydrates exists. Analysis of the phase-transition mechanism shows that some cages are maintained after the transition to the next clathrate structure, while others are recombined into different cages of the next structure. This is a novel mechanism that can be called "cage recombination mechanism." Low-temperature and high-pressure experiments have revealed that as the pressure increases, the guest molecules undergo a stepwise progression of orientational ordering, i.e., restriction of free rotation, which induces structural changes that stabilize the structure at high pressure. Theoretical studies have predicted that hydrogen-bond symmetrization in the host occurs at even higher pressures, further stabilizing the structure. Thus, hydrates respond to environmental changes such as pressure to achieve self-organization by the orientational ordering of the guest and hydrogen-bond symmetrization of the host. Additionally, results of high-temperature and high-pressure experiments conducted at conditions comparable to those in Neptune's ice mantle show that methane hydrate decomposes into solid methane and ice VII, both of which melt at further elevated temperatures. Then, the methane molecules undergo further molecular dissociation to form diamonds. These findings are valuable for modeling the interiors of icy planets and understanding how magnetic fields and heat are generated.

Keywords Methane hydrate, Hydrogen hydrate, High-pressure properties, High and low temperatures, Structural evolution, Transition mechanism, Guest orientational ordering, Molecular dissociation, Icy bodies, Diamond anvil cell (DAC)

*Correspondence:
Hisako Hirai
hirai@sci.ehime-u.ac.jp
Hirokazu Kadobayashi
kadobayashi@spring8.or.jp
[1] Geodynamics Research Center, Ehime University, 2-5 Bunkyo-Cho, Matsuyama, Ehime 790-8577, Japan
[2] Japan Synchrotron Radiation Research Institute, SPring-8, 1-1-1 Kouto, Sayo, Hyogo 679-5198, Japan

1 Introduction

1.1 Curious clathrate properties

In clathrate compounds, some atoms or molecules form polyhedral cages (referred to as the host) in which other atoms or molecules (referred to as the guest) are enclosed. Silicon and carbon atoms as well as water and silica molecules can all act as hosts. However, although the concept of carbon clathrates has been proposed

(Saito 1994), carbon clathrates have not yet synthesized. In clathrate hydrates, the host is a water molecule. This review focuses on clathrate hydrates. Fundamental knowledge regarding ice and hydrogen bonding can be found in classic studies and reviews (Franks and Rei 1973; Petrenko and Whitworth 1999). Water molecules have covalent bonds between their oxygen and hydrogen atoms, and the difference in the electronegativity of these two types of atoms results in the polarity of the molecule. Therefore, the hydrogen bonds formed by the water molecule develop a four-coordinate configuration. This configuration is strictly maintained, although the angles between the four hydrogen bonds show certain flexibility. Therefore, the overall shape that the molecule forms with its neighbors should be tetrahedral, even if distorted. For this reason, many types of structures can fill the three-dimensional space within the networks formed by water molecules while preserving the four-coordinate configuration, as seen in the polymorphism of water ice. Similarly, for clathrate hydrates, various polyhedral-based structures are formed.

In clathrates with different host species, polyhedral cages are formed by covalent or hydrogen bonding. These cages share individual faces to form the structure. Regardless of the host species or bond type, the structures are essentially identical. Such similar structures are formed supposedly because all of these host materials build stable structures by four-coordination. In silicon and carbon, such structures are formed by sp^3 hybridization orbitals, while in water molecules, such structures are formed due to molecular polarity. Meanwhile, the physical properties of the formed materials depend on the guest species and the bond type of the hosts. For example, silicon clathrates containing Ba atoms exhibit superconductivity (Kawaji et al. 1995) and have become a research hotspot in this field. While quartz (silica; SiO_2) is the most well-known mineral in mineralogy, it is less known that silica forms a structure nearly identical to that of methane hydrate (MH) (Kamb 1965), but with some modifications (Nakagawa et al. 2001; Yagi et al. 2007). Silica clathrate occurs naturally in the form of the mineral melanophlogite, which is found in hot springs and the structure of which traps gas molecules such as CO_2 and methane (Kamb 1965).

Clathrates are interesting materials because their properties originate from the fact that the host encapsulates the guest within its cage structure. The specific interaction potential within the cage results in characteristic guest motions and properties such as heat transfer, "rattling" (Nolas et al. 1996), and superconductivity (Kawaji et al. 1995). Clathrate hydrates also exhibit a characteristic property: When multiple guest molecules are captured in a cage, the intermolecular distances are extremely short. For instance, in the sII structure of hydrogen hydrate (HH), four hydrogen molecules are trapped in a 16-hedral cage (Mao et al. 2002; Lokshin et al. 2004). The intermolecular distance between the hydrogen molecules is 2.9 Å, which is significantly less than that (3.5 Å) in the low-pressure solid hydrogen phase I (hexagonal close-packed, hcp). In addition, the 20-hedral cages of MH-II (one of the high-pressure phases of MH) contain three to five methane molecules, and the intermolecular distances are relatively short (3.26–3.60 Å) (Loveday et al. 2001a, b; Tulk et al. 2012; Takeya et al. 2010) in comparison with the van der Waals diameter of methane molecules (4.2 Å). Furthermore, neutron and X-ray diffraction (XRD) studies have shown that these guests are dynamically disordered (Tulk et al. 2012; Takeya et al. 2010), in contrast with the static disorder found in minerals. The occupancy and distribution of guest molecules in the 20-hedral cage in MH-II are described in Sect. 2. These short intermolecular distances and dynamic behavior demonstrate the specificity of the environment in the cage.

Gas hydrates, such as MH, exhibit intriguing phenomena due to physical properties. In MH, methane and water molecules are separated from one another at ambient temperature and pressure owing to the hydrophobicity of methane despite their partial miscibility with each other. However, under certain conditions, methane molecules disperse easily and uniformly in the cage of water molecules, and they diffuse between cages or are dynamically distributed within a cage. In addition to the pressure–temperature conditions, this behavior is mainly related to the significant difference in gas solubilities and diffusion rates between the liquid phase and the ice or hydrate phase. Dyadin et al. (1994) reported that the solubility of hydrogen in ice Ih is much greater than that in water. This is because liquids have limited voids to incorporate gas molecules due to the random arrangement of water molecules, resulting in low solubility, whereas ice Ih has large voids due to its four-coordinated arrangement.

The diffusion and mobility of guests in ice and hydrates have been studied both experimentally and theoretically (e.g., Davidson 1973; Ripmeester et al. 1980; Ripmeester and Ratcliffe 1999; Davidson et al. 1983). Hydrogen molecules were reported to form a clathrate structure sII (Mao et al. 2002); later, Senadheera and Conradi (2007) investigated the diffusion of hydrogen molecules in this structure using nuclear magnetic resonance (NMR) under ambient pressure to discuss rotation and diffusion in large and small cages. This research direction was then followed by the development of high-pressure NMR techniques (Okuchi et al. 2007) to investigate the diffusion rate of hydrogen in filled-ice II (C1) and filled-ice Ic

(C2). The results reveal that the diffusion of guest hydrogen molecules occurs extremely rapidly, with a diffusion rate comparable to that of liquids. Such high diffusion and mobility in hydrates are due to the absence of chemical bonding between the host and guest with only weak interactions occurring between them. Nonpolar guests are stabilized in the cage by dispersive interactions. By contrast, oxides and silicates form structures with closely packed oxygen atoms. In such structures, the atoms are charge-constrained as anions and cations, and their mobility is lower than that of the atoms or molecules in hydrates. In the field of chemistry, several gas hydrates, including MH, have long been studied from the perspective of hydrophobic interactions. The basic concepts of hydrophobic interactions were described by Pratt and Chandler (1977), who developed a microscale theory to describe the structural and thermodynamic properties of infinitely dilute solutions of nonpolar solutes. By applying this concept to clathrate hydrates, several studies have attempted to understand the structures and properties produced by guest–guest and guest–host interactions in the cages. For example, Tulk et al. (2012) determined the number of guests and their statistical position within the large cage of MH-II from this viewpoint. Physical properties such as mechanical strength, elastic properties, thermal conductivity, thermal expansion, and dielectric constant of clathrate hydrates have attracted research interest (Ripmeester et al. 1994; Davidson et al. 1986), as summarized by Sloan (2007) and Sloan and Koh (2008). This review paper does not focus on these properties.

When clathrate hydrates are subjected to pressure and extremely high or low temperatures, they exhibit highly diverse physical properties. Gas hydrates undergo a wide range of structural changes when subjected to high pressure, as described in a subsequent section. Overviews of the structural changes as a function of guest size and pressure have been provided by our research group (Hirai et al. 2004) and others (Loveday and Nelmes 2008), and this topic is discussed in detail in Sect. 2. Additionally, it has been discovered that the transition between clathrates occurs via a characteristic mechanism (Hirai et al. 2015), which is discussed in Sect. 3. After the cage structure collapses under extreme pressure, the gas hydrate forms a filled-ice structure, which takes the ice structure as its host framework. Ice is known to undergo hydrogen-bond symmetrization under high pressure (e.g., Aoki et al. 1996; Goncharov et al. 1996), whereas water molecules undergo proton ordering at low temperatures (Salzmann et al. 2009a, b). Theoretical studies have proposed similar phenomena for the host framework of gas hydrates. Predictions of hydrogen-bond symmetrization for MH have been reported (Iitaka and Ebisuzaki 2003; Schaack et al. 2019, 2020) but have not yet been verified experimentally. Proton ordering of ice has been studied experimentally via doping studies and theoretical calculations at low temperatures (e.g., Salzmann et al. 2009a). For HH, Zhang et al. (2012) used first-principles calculations to prove that proton ordering occurs at temperatures below 9 K in pure HH. Owing to the presence of guests in the hydrate ice framework, hydrogen-bond symmetrization and proton ordering of the framework can occur under conditions different from those found in pure water ice structures; consequently, the material properties may differ significantly. Furthermore, because the guest is surrounded by the host, its behavior differs from that of molecular crystals, such as solid methane and hydrogen, which are composed solely of the guest species.

Guest rotation is expected to be suppressed, resulting in molecular distortion and structural changes at high pressures or low temperatures. The restriction of the free rotation of guest molecules, which fixes their orientation, is referred to as orientational ordering. The orientational ordering of molecular rotation in molecular crystals and hydrates is described in Sects. 4 and 5. The ordered states of guests in certain phases have not yet been fully explained by experiments or quantum theory. However, in this review, orientational ordering is described by a classical treatment. Notably, orientational ordering occurs even in hydrate structures in which the guest is affected by the host. The conditions under which this ordering occurs depend on the degree of effect, that is, the strength and properties of host–guest interactions, which differ from those found in the corresponding molecular crystals of the guest species. Additionally, the behavior of gas hydrates at elevated temperatures and pressures has attracted research interest. The current aim is to determine whether MH can withstand extremely high temperatures or whether it simply melts, decomposes into high-pressure ice and guest solids, or forms a new high-pressure phase. This topic is discussed in Sect. 6.

MH is called "burning ice" and is attracting attention as a potential next-generation energy source. However, it has inherent global warming potential because of the risk of methane release (e.g., Kvenvolden 1998). As such, MH is a relevant material for contemporary global environmental and energy resource issues. MH reportedly played a role in past environmental changes, such as the recovery from "snowball Earth" in the Neoproterozoic era (e.g., Zhao et al. 2021), the warming that led to the mass extinction in the Permian–Triassic boundary (e.g., Burger et al. 2019), and glacial–interglacial climate changes (e.g., Deng et al. 2021). Based on experiments, theoretical calculations, and spacecraft measurements, MH has been predicted to exist widely in the solar system

beyond the Earth (e.g., Mao et al. 2007). For example, the presence of MH in the ice mantle of Saturn's moon Titan was proposed based on the thermodynamic conditions necessary for its existence, where MH could be a possible source of atmospheric methane (Loveday et al. 2001a, b). The presence of hydrocarbon hydrates in the interior of Enceladus (another moon of Saturn) was predicted based on an analysis of the plume ejections measured by the Cassini spacecraft (Kieffer et al. 2006). In addition, the thermodynamic conditions inside short-period comets (Halley-type comets) allow for the presence of clathrate hydrates (Marboeuf et al. 2010). Furthermore, MH was thought to have been the primary methane-containing phase in the nebulae from which Saturn, Uranus, Neptune, and their major satellites were formed (Lunine and Stevenson 1987). Meanwhile, HH is also attracting interest as a potential hydrogen-storage material for enabling the widespread use of hydrogen energy (Mao and Mao 2004; Lee et al. 2005; Struzhkin et al. 2007). Furthermore, HH may act as a hydrogen carrier during the early stages of stellar formation, i.e., protostars (Sandford et al. 1993). Under suitable temperature–pressure conditions, both MH and HH are expected to exist on icy planets and satellites, as well as newly discovered exoplanets and to exhibit a range of physical properties.

We have been investigating how pressure and temperature changes affect the physical properties of hydrates to obtain insight into their physical properties. The elucidation of high-pressure properties is important for materials science and is similarly critical to planetary science. In the current review, we discuss their high-pressure structural changes at ambient temperature (Sect. 2), transition mechanism (Sect. 3), low-temperature high-pressure properties (Sect. 4), structural evolution (Sect. 5), and high-temperature high-pressure properties (Sect. 6).

2 Phase changes of gas hydrates under high pressures

2.1 Crystal structures of gas hydrates

Numerous guest species form clathrate structures, many of which form one of three structures, namely cubic sI, cubic sII, or hexagonal sH, depending on the guest size at ambient-to-low pressures (Sloan and Koh 2008; Jeffrey 1984; Dyadin et al. 1999; Davidson et al. 1984a, b). The crystal structures of sI (McMullan and Jeffrey 1965), sII (Mak and McMullan 1965), and sH (Ripmeester et al. 1987; Udachin et al. 1997) were previously determined. The sI structure is composed of two regular dodecahedra and six tetradecahedra. sII is composed of 16 regular dodecahedra and 8 hexadecahedra. sH is composed of one icosahedron, three regular dodecahedra, and two modified dodecahedra. Hereafter, a dodecahedron, tetradecahedron, hexadecahedron, and icosahedron are referred to as 12-hedron, 14-hedron, 16-hedron, and 20-hedron, respectively (Sloan and Koh 2008).

When 12-hedra are regarded as small cages and 14-hedra, 16-hedra, and 20-hedra are regarded as large cages, the ratios of large to small cages in the sI, sII, and sH structures are 3:1, 1:2, and 1:5, respectively. This ratio is an important factor that controls the structure formation and high-pressure phase transition, i.e., smaller guests form the sII structure, which is dominated by small cages. As the size of the guest increases, the sI structure is formed, followed by the sH structure. On the left side in Fig. 1, the initial structure of clathrate hydrates under ambient pressure is depicted as a function of guest size. In this figure, hydrophobic guests are shown except for hydrogen. The largest guest shown is ethane (C_2H_6). For guests larger than ethane, the sII structure is formed again, allowing larger guests to enter the 16-hedra. When the guest is even larger (e.g., methylcyclohexane), the sH structure is formed, allowing it to enter the 20-hedron. This guest size-dependent structure under ambient pressure has been described by Sloan and Koh (2008). Under high pressure, structures that can efficiently accommodate more guest molecules are formed (Mao et al. 2007).

2.2 General rule of phase transitions under high pressure

Since the pioneering study by Dyadin et al. (1997), many high-pressure studies have been published. A general rule of phase transitions in clathrate hydrates can be deduced from Fig. 1 (Hirai et al. 2004, 2008a, 2014; Loveday and Nelmes 2008; Hirai 2009). In general, the initial structure of sI or sII changes to sH with increasing pressure (e.g., Hirai et al. 2001; Loveday 2001a; Chou et al. 2000; Shimizu et al. 2002). With increasing pressure, the sII structure with a small guest first transforms into the sH structure and then another cage structure (tetragonal sT) (Kurnosov et al. 2001; Hirai et al. 2002a, b). The sT structure is composed of only 20-hedra, which differ from those found in sH. Small guests are tightly packed into the 20-hedra with double occupancy (Manakov et al. 2009; Kuhs et al. 1997; Itoh et al. 2001). Thus, smaller guests can enter the cage structure because multiple occupancy is possible (Kuhs et al. 2018). In sH as the initial structure under low pressure, the 20-hedron is occupied by a single large guest, whereas in sH formed after a phase transition under high pressure, the 20-hedron is multiply occupied by smaller guests, such as methane molecules. The number of guests (occupancy) and their dynamic distribution in the 20-hedral cage in MH-II have been elucidated by neutron experiments (Tulk et al. 2012), Raman spectroscopy (Shimizu et al. 2002), and a newly developed XRD method (Takeya et al. 2010). Guest occupancy of 3–5 molecules has been proposed, but the debate regarding the number of molecules continues.

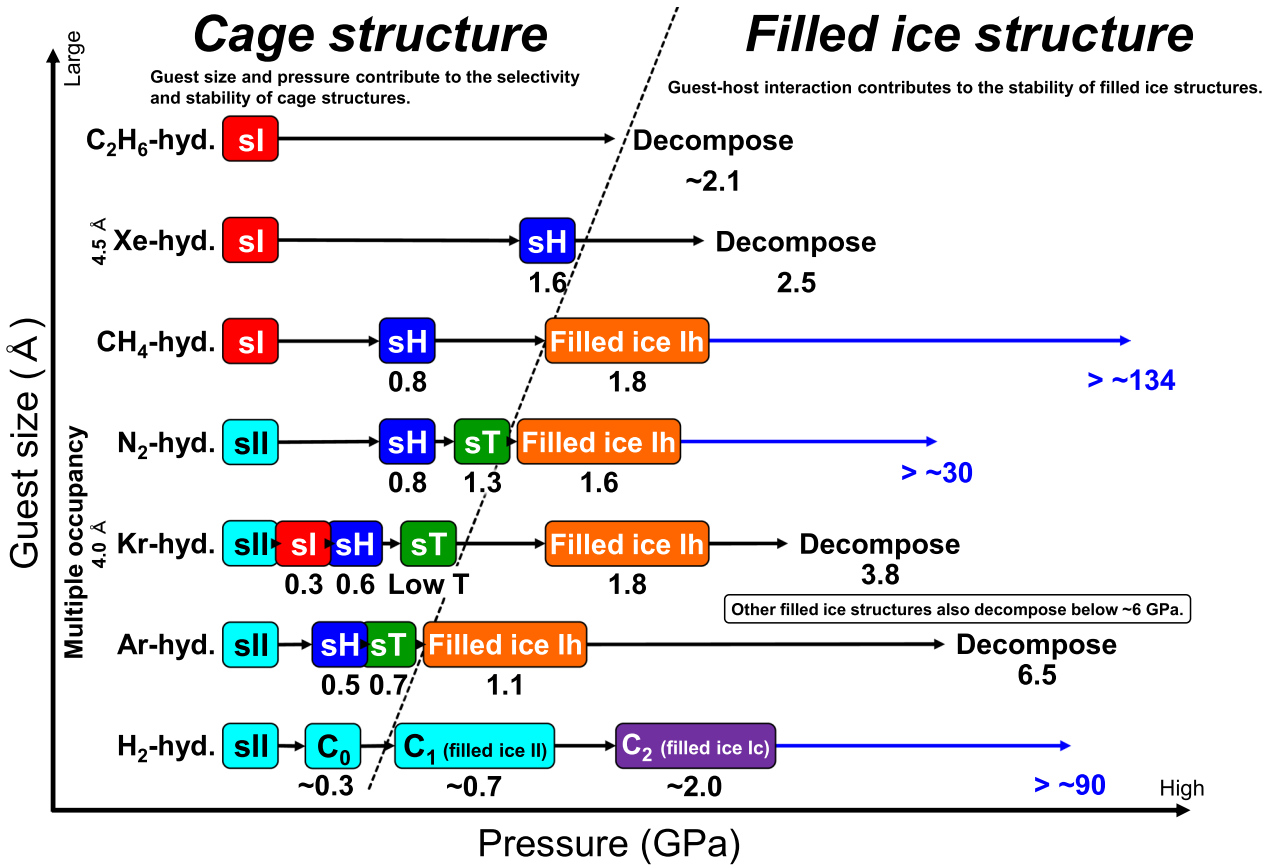

Fig. 1 General trends in the phase changes of gas hydrates as a function of pressure and guest size. The vertical axis indicates the guest size, with hydrogen being the smallest guest and ethane being the largest guest. Hydrates with guests larger than ethane have an initial sII structure, while extremely large guests result in an initial sH structure. The horizontal axis indicates pressure. Only MH and HH exhibit outstanding high-pressure stability

Regarding multi-occupancy of cages, Kuhs et al. (1997) performed precise neutron diffraction experiments with N_2 hydrate and quantified the position and occupancy of guest molecules in large and small cages, especially the double occupancy of N_2 molecules in large cages, for the first time. They also discussed the relationship between occupancy and compressibility. Subsequently, multiple occupancy was discussed for large cages of sII in Ar hydrate (Itoh et al. 2001).

As illustrated in Fig. 1, in each sI, sII, and sH structure, the structure containing the larger guest is maintained up to a higher pressure. Thus, the guest can support the cage structure; that is, the cage structure is sustained through the specific interaction between the guest and host. As discussed in a later section, transitions between cage structures depend on the pressure, guest size, and chemistry. As the cages are compressed to their limit, the initial structure is converted into a more stable cage structure that can more efficiently accommodate the guest under high pressure. Under even higher pressures, the cage structure eventually collapses mainly because of the limitation in the balance between the host–guest interaction that maintains the cage structure due to the decreasing intermolecular distance forced by the pressure. Gas hydrates were initially believed to be unstable under high pressure, but high-pressure experiments revealed the existence of newly discovered hydrate structures under high pressure. The high-pressure structures are called filled-ice structures because their fundamental framework is an ice structure with voids filled with guests. Two filled-ice structures were previously reported, with frameworks denoted as ice II and ice Ic. First, a structure containing helium atoms in the voids of the ice II framework was reported (Londono et al. 1988), followed by structures containing hydrogen molecules in the voids of the ice II and ice Ic frameworks as compounds C1 and C2, respectively (Vos et al. 1993, 1996). The bulk compositions of C1 and C2 are $H_2/H_2O = 1{:}6$ and 1:1, respectively. The filled-ice Ic structure, C2, is understood as follows. The structure of Ice VII is composed of

two interpenetrating ice Ic frameworks, whereas in C2, hydrogen molecules replace the water molecules in one ice Ic framework. C1 and C2 were recognized as novel compounds composed of molecular hydrogen and water molecules. A study on the high-pressure phase of MH discovered a new filled-ice structure, namely filled-ice Ih (Loveday et al. 2001a). Although this structure appeared to be similar to the ice Ih framework, the two structures are fundamentally different. The framework contains channel-like voids that are filled with methane molecules, with a bulk composition of $CH_4/H_2O = 1{:}2$, indicating a notably methane-rich phase (Loveday et al. 2001b).

After forming a unique filled-ice structure, hydrates undergo a new phase-transition pathway. Only a few guests can form filled-ice structures because of a restriction in guest size (e.g., Hirai et al. 2006). Most filled-ice structures are stable up to a pressure of ~ 6 GPa, above which they begin to decompose. Meanwhile, MH and HH filled-ice structures have been experimentally observed to maintain their fundamental structure under pressures of at least 134 (Kadobayashi et al. 2020a; Machida et al. 2006) and 90 GPa (Machida et al. 2008), respectively. The reason for the outstanding stability of these hydrates will be described in Sects. 4 and 5. A N_2-hydrate filled-ice structure was able to withstand pressures of up to 30 GPa (Loveday and Nelmes 2008); however, the reason for this stability was unclear. Another study on a N_2–H_2O system by Raman spectroscopy and XRD up to 140 GPa identified a fine-grained state above 6 GPa, but the detail of the state has not been elucidated (Zhang et al. 2021). The names of the high-pressure phases of MH that have been widely used in high-pressure research are as follows: The initial MH structure sI is referred to as MH-I; the sH structure above 0.9 GPa as MH-II; and the filled-ice Ih structure above 1.8 GPa as MH-III. Throughout this paper, we use this nomenclature in the text and in Figs. 2, 3, and 4.

Studies on the behavior on MH and HH under ultra-high pressure were conducted theoretically and experimentally. In our previous experiment, another high-pressure phase above MH-III (hereafter called MH-IV but was denoted by HP1 in previous papers) was observed; in subsequently performed experiments up to 134 GPa, the space group of MH-IV was shown to be Pmcn, and the precise formation pressure of MH-IV was determined to be 34 GPa (Kadobayashi et al. 2020). Schaack et al. (2019) also reported a space group (Pmcn) and the XRD patterns of the MH-IV structure by ab initio calculations and Raman spectroscopy. Their results are consistent with our findings and previously published XRD patterns (Tanaka et al. 2013). As for hydrogen-bond symmetrization in MH by theoretical calculations, the symmetrization pressures differed among these studies. Iitaka and Ebisuzaki (2003) reported a pressure of 70–80 GPa with the assumption that MH-III was maintained up to a high pressure, while Schaack et al. (2019) reported two values, namely 30 GPa in MH-III and 50 GPa in MH-IV. Schaack et al. (2019) also measured the Raman spectra up to 150 GPa and demonstrated that symmetrization occurred twice at 30 in MH-III and 50 GPa in MH-IV; however, this may not be sufficient experimental verification of the theoretical predictions. In addition, in our experimental studies, we were unable to observe changes in the diffraction lines or slope of the volume versus pressure curves under the pressures predicted by these theoretical studies. To date, no experimental validation of these theoretical predictions has been reported. Therefore, further studies should focus on confirming symmetrization experimentally using neutron diffraction and Raman spectroscopy as well as on determining the detailed crystal structure. The symmetrization of water ice (VII–X transition) has been experimentally verified to occur at ~ 60 GPa (Aoki et al. 1996; Goncharov et al. 1996), and the details of the symmetrization process have been discussed considering the results of XRD and first-principles calculations (Sugimura et al. 2008). The difference in symmetrization pressure between ice VII and MH could be attributed to differences in the host ice frameworks, interactions, and physical properties originating from the presence of guest molecules.

The ratios of CH_4/H_2O in the sI, sII, sH, sT, and filled-ice Ih structures are 8:46, 24:136, 6–10:34 (due to variable occupancy of the 20-hedron), 4:12, and 4:8, respectively (Jeffrey 1984; Sloan and Koh 2008). Gas hydrates release water upon these phase transitions, resulting in a higher guest content. Because clathrate hydrates are non-stoichiometric compounds, the compositions of natural and synthesized samples do not agree with the methane/water ratios given above. Therefore, the composition of samples used in experiments should be determined prior to conducting the experiments. The bulk compositions of the samples used in our high-pressure study of MH were estimated as follows. The starting material MH-I was synthesized by an ice–gas interface method, and gas chromatography and combustion measurements that were conducted before the high-pressure experiments indicated an occupancy of 95–97% ($CH_4/H_2O = 1{:}\sim 5.7$). The starting material with this composition was loaded into a diamond anvil cell (DAC) and compressed. Direct measurement of the composition of the high-pressure phase after phase transition in the DAC is difficult. The water component is released during two transition

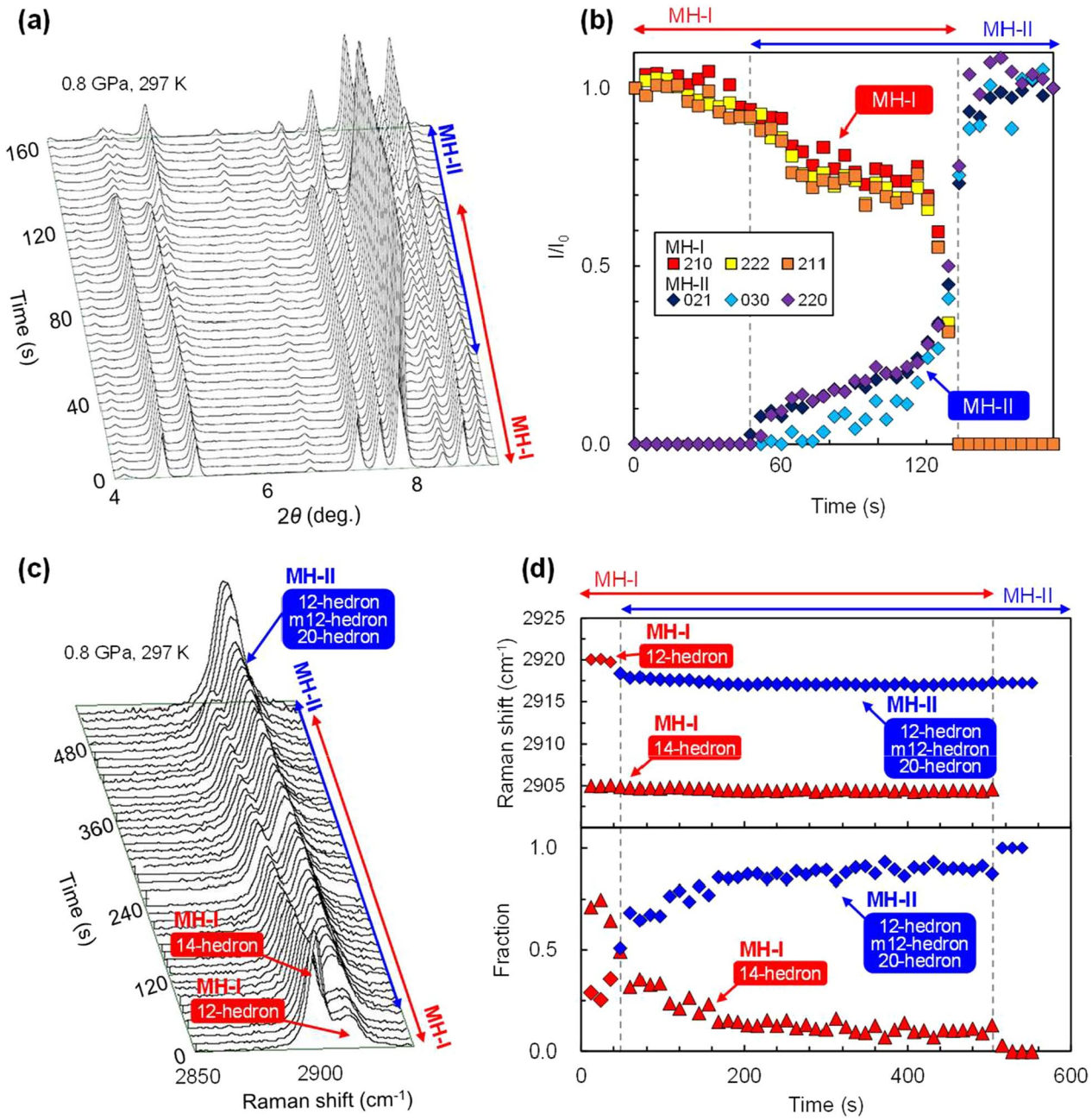

Fig. 2 Progression of the phase change from MH-I to MH-II as described by changes in the host structure and vibrational modes of the guest over time. **a** Time-resolved XRD patterns and **b** relative intensity of the representative diffraction lines of MH-I and MH-II. **c** Time-resolved Raman spectra of vibration modes and **d** (top) Raman shift and (bottom) fraction of methane molecules in each cage in MH-I and MH-II. The 12-hedra in MH-I are preserved in the following MH-II structure, and the 14-hedra of MH-I are recombined into 12-hedra, modified 12-hedra, and 20-hedra in MH-II. This figure is modified from Hirai et al. (2015)

steps, but all of the methane is incorporated into the next structure; therefore, the composition of MH-III is assumed to be $CH_4/H_2O = 1{:}2$. The released water component is converted into ice VI and VII during subsequent compression, and MH coexists with ice.

2.3 Effect of the guest chemical properties on cage stability

Figure 1 depicts the phase change only for hydrophobic guests. The chemical properties of the guest have a significant effect on the stability of the cage structure. According to Jeffrey and McMullan (1967) and Jeffrey

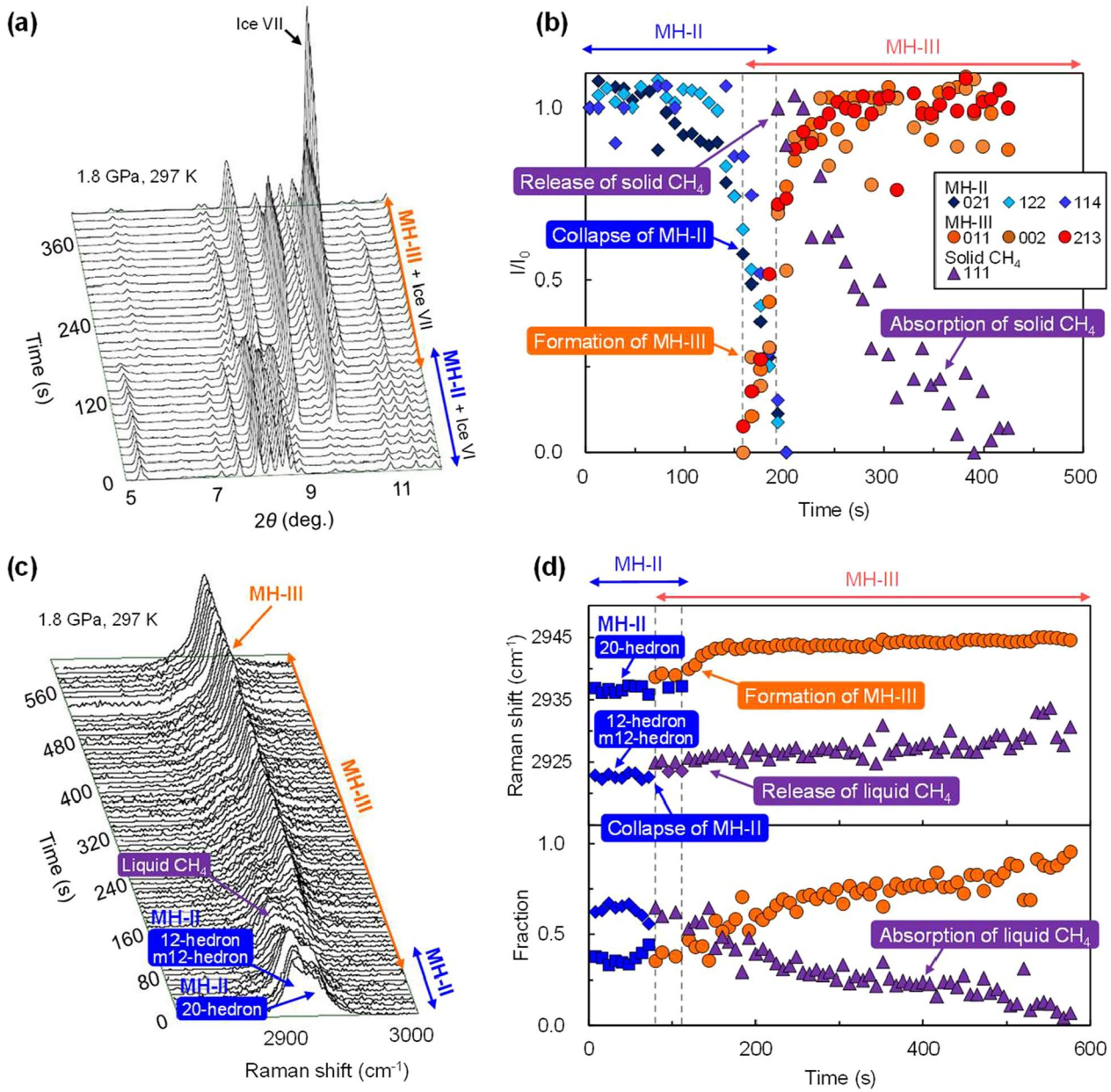

Fig. 3 Progression of phase change from MH-II to MH-III as described by changes in the host structures and vibrational modes of the guests over time. **a** Time-resolved XRD pattern and **b** relative intensity of the representative diffraction lines of MH-II and MH-III. **c** Time-resolved Raman spectra and **d** (top) Raman shift and (bottom) fraction of methane molecules in each cage of MH-II and MH-III and released liquid methane. The data show that MH-II collapses abruptly and that MH-III is reconstructed. This figure is modified from Hirai et al. (2015)

(1984), guest molecules are classified into four groups: (1) hydrophobic compounds, (2) water-soluble acid gases, (3) water-soluble polar compounds, and (4) water-soluble ternary or quaternary alkylammonium salts. The physicochemical properties of the guest molecules incorporated into hydrates have been investigated mainly by NMR (e.g., Davidson et al. 1984a, b), XRD, and neutron diffraction (Udachin et al. 2002). Some guest types are located outside the center of the cage, which affects the hydrate stability (Kirchner et al. 2004).

CO_2 is a typical water-soluble acidic gas. Because CO_2 and CH_4 molecules have a similar size as guests, CO_2 hydrate has the same initial structure as MH. However, even under high pressure, CO_2 hydrate cannot exist at ambient temperature, and its stability region differs from that of MH (Hirai et al. 2010; Manakov et al.

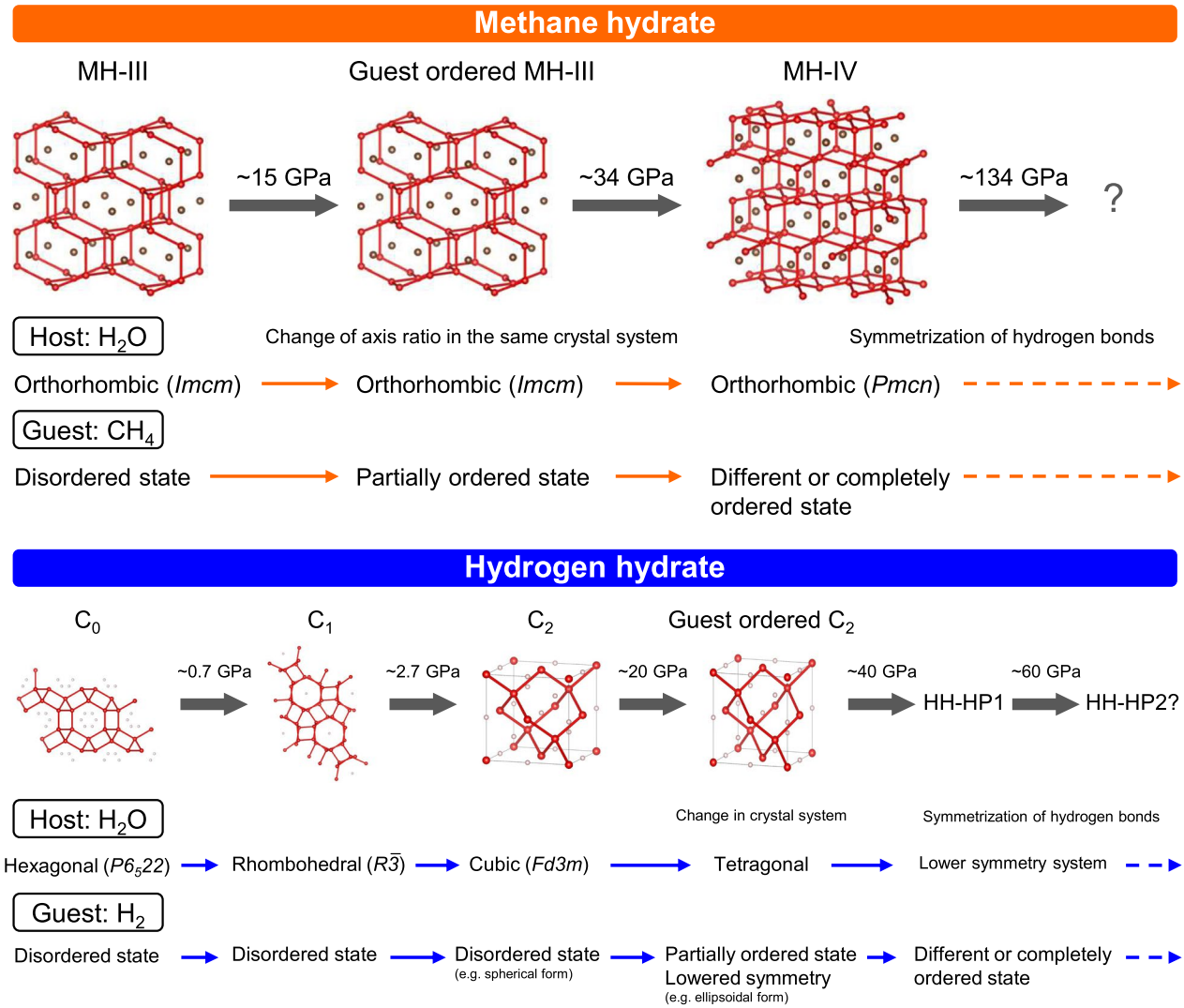

Fig. 4 An overview of the structural evolution of (top) MH and (bottom) HH after transition to the filled-ice structure, except for HH-C0. With increasing pressure, the guests undergo stepwise orientational ordering accompanied by structural changes. Hydrogen-bond symmetrization of the host was predicted to occurs at even higher pressures (further changing the structure), although this has not yet been fully verified experimentally

2009). The decomposition curve of MH has a positive slope with respect to temperature and pressure, whereas that of CO_2 hydrate has a positive slope up to a certain inflection point, after which the slope becomes negative (Nakano et al. 1998; Tulk et al. 2014); this indicates that CO_2 hydrate can exist only at low temperatures. We performed experiments with CO_2 hydrate at low temperatures and under high pressures using a helium-refrigerated cryostat in the pressure and temperature ranges of 0.2–3.0 GPa and 280–80 K, respectively (Hirai et al. 2010). We clarified the phase transitions in this low-temperature region and discussed the cause of the instability of CO_2 hydrate. Tulk et al. (2014) reported that CO_2 formed the filled-ice Ih structure at low temperatures and under high pressures, which was also observed in our experiments as a HP phase. The formation of CO_2 filled-ice Ih structure may be ascribed to the fact that guest–host interactions that destabilize the structure at room temperature are weakened at lower temperatures.

Because the methane molecule is typically hydrophobic and experiences repulsive interaction with the water molecules of the cage, it rotates to stay as far away from the water cage as possible, that is, approximately in the cage center. By contrast, the distribution of guest CO_2 in a water cage is different. Alavi et al. (2008) reported the dynamic distribution of guest CO_2 molecules at different

temperatures (77–238 K) using molecular dynamics simulations and NMR experiments. Takeya et al (2010) reported broad dynamic distributions of CO_2 guest molecules near the equatorial plane of cages by XRD study, and Ikeda et al. (1999) showed a large temperature factor based on neutron diffraction studies. For a hydrate with guest tetrahydrofuran (THF), a typical hydrophilic substance, Alavi et al. (2009) showed that an instantaneous hydrogen bond was formed between the guest oxygen atom of THF and the host water molecule, which caused a defect in the adjacent water molecule. This process supposedly affected the dynamics of the water molecule and the instability of hydrogen bonds. As for CO_2 hydrate, instantaneous hydrogen bonding with the host has not been reported. However, considering the dynamic distribution of the guest molecules, interaction with the host may be further enhanced under high pressure and at high temperature (~300 K), which may be a potential source of the instability of the CO_2 hydrate.

Hydrophilic guests, such as cyclic ethers belonging to the water-soluble polar compound group like ethylene oxide and THF, form hydrates at ambient temperature and pressure and have been the subject of much research. Oxygen atoms in cyclic ethers promote defect formation in host water molecules (Davidson et al. 1984a, b). When the hydrophilicity of the guest increases, it forms a semi-clathrate structure, where permanent rather than instantaneous host–guest hydrogen bonds are formed, thereby resulting in significant distortion of the cage (Jeffrey 1984, 1969; Davidson 1973).

CO_2 hydrate has been found on the Earth's ocean floor (Sakai et al. 1990). In addition, given the global challenge of reducing atmospheric CO_2 levels to prevent climate change, the use of CO_2 hydrates for sequestering CO_2 in the ocean has been proposed (Ohgaki et al. 1996). CO_2 hydrate is predicted to exist beneath the permafrost on Mars and is one of the most important hydrates in planetary science (Pellenbarg et al. 2003).

3 Phase-transition mechanism

3.1 Research from phase transitions to transition mechanisms

In addition to the variety of structure and structural changes of gas hydrates described up to this point, the dynamics and mechanism of the transition are of considerable interest. To date, studies on the dynamic processes of gas hydrate formation, decomposition, and phase transformation have been extensively conducted using in situ spectroscopy methods. For example, the kinetics of the displacement of CH_4 with CO_2 and N_2 gas in MH prepared in a porous silica gel matrix were investigated by in situ NMR spectroscopy (Cha et al. 2015). The relative mobility of guest and host molecules in MH film was determined using isotopic tracers and time-dependent Raman spectroscopy (Davies et al. 2010). In addition, the formation and phase-change behavior of methane-based multi-component gas hydrates were studied using in situ microscopy, Raman spectroscopy, and XRD (Schicks et al. 2006). However, studies on the dynamics and mechanism of the transitions among the three phases of MH are limited (Chen and Yoo 2012; Ikeda and Terakura 2003). The formation and phase-transition mechanisms of MH under dynamic compression conditions and the kinetics as a function of compression rate were studied using Raman spectroscopy (Chen and Yoo 2012). Furthermore, the phase-transition mechanism under a fixed pressure for the MH-I to MH-II and MH-II to MH-III transitions was investigated by our group (Hirai et al. 2015; Kadobayashi et al. 2017).

The phase change occurs through a displacive (the word "martensitic" is used in this review as it is used in metallurgy) mechanism, which does not involve atomic diffusion or a reconstructive mechanism but involves diffusion on a broad scale. A martensitic transition is characterized by a shift or rotation of some atoms in the structure to the next structure, i.e., the structures before and after the transition have a certain crystallographic relationship. By contrast, no structural relationship exists before and after the transition in transition via reconstructive mechanisms. Because gas hydrates consist of the guest and host, we assume that the transition mechanism is not as simple as those described above. In particular, the changing process of individual cages during phase transition is not yet well understood.

3.2 Transition mechanisms of MH by time-resolved analyses

MH-I transforms to MH-II under 0.8 GPa and further transforms to MH-III of a filled-ice Ih structure under 1.8 GPa. Our previous studies (Hirai et al. 2015; Kadobayashi et al. 2017) were conducted under a fixed pressure and at ambient temperature using time-resolved XRD and Raman spectroscopy, and a charge-coupled device (CCD) camera was synchronized with XRD to examine the changes in the framework formed by water molecules and the change in the cage containing methane molecules. The bulk composition of the sample was described beforehand.

For the MH-I to MH-II transition, Fig. 2a, b shows the time-resolved XRD patterns and relative intensities of the MH-I and MH-II diffraction lines with strong intensity and without superimposition under a fixed pressure of 0.8 GPa. The inverse correlation observed between the intensities of MH-I and MH-II indicates that the structural framework gradually transforms from MH-I to MH-II. Figure 2c shows the change in

the C–H vibrational modes of methane in individual cages as observed by time-resolved Raman spectroscopy under 0.8 GPa. The intensity of the vibration mode of the 14-hedra decreased over time and eventually disappeared, whereas the vibration mode of the 12-hedra of MH-I was observed both during and after transition (Fig. 2c). With decreasing intensity of the 14-hedra of MH-I, the intensities of vibration modes of 20-hedron, modified 12-hedra, and 12-hedra of MH-II became stronger. The vibrational modes from the three cages in MH-II overlapped, but the assignments of modes to individual cages were consistent with those in previous reports (Sasaki et al. 2007; Shimizu et al. 2002). Evidently, additional 12-hedra, modified 12-hedra, and 20-hedra of MH-II are formed from the 14-hedra of MH-I, whereas the 12-hedra of MH-I remains unchanged after transition. The change in the Raman shift of the C–H modes for each cage is shown in Fig. 2d (top) as a function of time, whereas Fig. 2d (bottom) shows the change in the relative fraction of each cage. The fraction of 14-hedra gradually decreases over time, whereas that of the 12-hedra + modified 12-hedra + 20-hedra gradually increases in inverse proportion. Importantly, although the 14-hedra in MH-I change to the three types of MH-II cages, the Raman shift of 14-hedra remains unchanged during the transition [Fig. 2d (top)]. Therefore, any 14-hedra that remain during the transition exist as complete individual cages, and their replacement by the three types of MH-II cages must be sequential. As seen from the CCD camera image, the progress of transition can be directly observed. We saw that transition started at many different positions in the sample chamber and gradually spread. Although both MH-I and MH-II were transparent to visible light, they were distinguished by their different refractive index values (Hirai et al. 2015).

For the MH-II to MH-III transition, Fig. 3a shows the time-resolved XRD patterns under 1.8 GPa, and Fig. 3b shows the relative intensity of the diffraction lines of the MH-II and MH-III and solid methane as a function of time. After some time, MH-II abruptly disappeared, and the MH-III framework formed quickly. Solid methane was also identified at this point, albeit with a faint XRD intensity. Solid and liquid methane were released upon the collapse of MH-II. Under the transition conditions of 1.8 GPa and ambient temperature, methane is solid (Hazen et al. 1980), but not all of the released methane can be solidified within the experimental time. The weak XRD peak for solid methane indicates its presence at low concentration, while the larger fraction of liquid methane was quantified by Raman spectroscopy. Thus, the time-resolved XRD data reveal that the collapse of the MH-II structure is accompanied by the formation of the MH-III framework. The time-resolved Raman spectra of the C–H vibrational modes during the phase transition at 1.8 GPa are shown in Fig. 3c. The Raman shifts of the C–H modes of the MH-II cages, MH-III, and liquid methane are shown in Fig. 3d (top), and the relative fraction of individual methane molecules is shown in Fig. 3d (bottom). The Raman data also indicate the rapid collapse of MH-II, simultaneous appearance of liquid methane and MH-III formation, and decrease in the fraction of liquid methane with a corresponding increase in the fraction of methane in MH-III, which suggest that MH-III is completed sequentially. In this transition, a drastic change in the sample was captured by the CCD camera. The transparent MH-II in the sample chamber changed color abruptly from brown to black, indicating the release of either liquid or solid methane, and accordingly, the complete collapse of MH-II. We have shown that when methane molecules are released through MH collapse, the sample turns brownish to black. This change is most likely due to light scattering at the grain boundaries (Hirai et al. 2015). As for determining solid and liquid methane and methane molecules within MH-III by Raman spectroscopy, we have accumulated data on changes in the vibrational mode with pressure change for the three phases (Kadobayashi et al. 2018, 2020b). Based on the data, the three methane phases can be clearly distinguished.

3.3 Characteristic transition mechanisms of clathrate hydrates

The MH-I to MH-II transition is characterized by the retention of the 12-hedra and the replacement of the 14-hedra by the three types of MH-II cages. Although a portion of the structure is retained, this transition is not applicable to the martensitic transition. Additionally, the change in composition and the inverse correlation in the XRD and Raman intensity are not consistent with properties of martensitic transition. Therefore, we defined this transition between cage structures as a "cage recombination transition" (Hirai et al. 2015). The similar inverse correlation between XRD and Raman intensity changes indicates that both host cage recombination and methane migration proceed gradually. However, the details regarding how oxygen atoms move to form new cages and how methane molecules move from old cages to new cages remain unclear. Our XRD, Raman, and CCD camera observations revealed that during the MH-II to MH-III transition, MH-II completely decomposed and released methane, and then, the MH-III framework was formed quickly. This was followed by the gradual absorption of released liquid and solid methane to complete the MH-III structure. These findings imply that this transition can be viewed as a typical reconstructive mechanism accompanied by diffusion. The reconstructive mechanism is reasonable because it is a transition from a cage

structure to a fundamentally different filled-ice structure, and the chemical composition (water-to-methane ratio) changes significantly.

Under static compression (fixed pressure), the time taken to complete the MH-I to MH-II and MH-II to MH-III transitions differs. The XRD results indicated changes of the structural framework, with a timescale of ~ 50 to 60 s for both transitions. The Raman results indicated the migration of guests between cages in the transition from MH-I to MH-II and from outside into the framework in the transition from MH-II to MH-III. The time required for 80% of the transition to be completed was 120 s for MH-I to MH-II and 400 s for MH-II to MH-III. The end point of completion is difficult to exactly determine in both transitions, but the MH-II to MH-III transition evidently took much longer than the former MH-I to MH-II transition. The times required for framework formation in both transitions are similar, whereas those required for the guest migration to finalize the structure are different. This outcome suggests that the rate at which guest molecules move through the solid between cages is higher than that at which guest molecules outside the framework move through the liquid and into the framework. The distinct kinetics of the transitions are reasonable considering that the transition from MH-I to MH-II occurs via cage recombination in solid, whereas that from MM-II to MH-III occurs via a reconstructive mechanism. Our experiments revealed a characteristic property that the host and guest acted separately and at different rates, regardless of the transition mechanism (Hirai et al. 2015; Kadobayashi et al. 2017). A future challenge is to determine the specific molecular movements during guest migration and host cage recombination. In addition, the transition mechanisms of other hydrates, particularly those with different initial structures and transition paths, have not been studied. The findings of such studies are expected to provide a more complete picture of the transition mechanism of gas hydrates.

4 Low-temperature properties

4.1 Phase transition induced by guest orientational ordering

In clathrate hydrates, guests rotate around the center of the cage or are dynamically disordered over a certain area of the cage, maintaining their own unique interaction with the host. Their behavior depends on chemical properties such as hydrophobicity or hydrophilicity (Davidson et al. 1984a, b; Kirchner et al. 2004; Udachin et al. 2002). Such guest rotation also occurs in filled-ice structures (e.g., Okuchi et al. 2007). During our investigation of room-temperature properties (e.g., Hirai et al. 2006), we hypothesized that the rotation of the guest molecules in the filled-ice structure would be suppressed under high pressure and at low temperature and that the orientational ordering of the guests would occur in a stepwise manner. This idea is based on the knowledge that orientation ordering proceeds in a stepwise manner in molecular crystals such as solid methane (e.g., Bykov et al. 2021; Bini and Pratesi 1997) and solid hydrogen (e.g., Mao and Hemley 1994). The basic quantum behavior of molecular rotation mainly in solid hydrogen has been described previously (e.g., Hemley and Mao 1996; Silvera and Dias 2021). Molecules have quantized rotational energy levels that are disturbed by the interaction potential of the local environment. In free rotators, the rotational state can be disturbed, and the energy level splits. For the HH clathrate structure, the splitting of rotational energy levels and restriction of molecular rotation have been described in detail by Strobel et al. (2009), as discussed in Sect. 4.3. The present review does not discuss quantum theory and explores the concept of ordering using only a classical approach. For example, such rotation-restricted states are qualitatively described as orientationally ordered or rotation-restricted states. The splitting of rotational levels is observed as the splitting of the roton mode in the Raman spectra; therefore, ordered or rotation-restricted states can be observed by Raman spectroscopy.

The rotational state of solid hydrogen has been comprehensively studied by infrared (IR) and Raman spectroscopy, which have revealed the existence of three crystalline phases solid hydrogen, I, II, and III, and rotational ordering, symmetry breaking, and the resulting structures have been discussed (e.g., Mazin et al. 1997; Hanfland et al. 1993). According to these studies, phase I is a low-pressure orientationally disordered phase with an hcp structure, which at cryogenic temperatures changes continuously to phase III via the intermediate phase II under approximately 160 GPa (Mao and Hemley 1994). Phase III strongly absorbs an IR-active vibron (Hanfland et al. 1993), and a considerable discontinuous reduction in the Raman vibron frequency is observed (Lorenzana et al. 1989). Based on these optical behaviors, phase III is a classically orientational-ordered phase. The transition from phase II to phase III is considered to be a transition from the ordering of the angular momentum state of hydrogen molecules to the classical orientational ordering of rotating hydrogen molecules (Mazin et al 1997). Based on this knowledge, structural models for phases I, II, and III have been proposed (Toledano et al. 2009; Hemley 2010). According to these studies, Phase I is a disordered phase with hcp space group $P6_3/mmc$. Phase II is a partially ordered phase with broken symmetry and space group Cmcm. Phase III is a fully ordered structure with the space group $Cmc2_1$. A synchrotron XRD study has also reported that phase III is consistent with the spectroscopically proposed features of the

classical orientational ordering of rotating hydrogen molecules (Akahama et al. 2010). Therefore, phase III is classically regarded as an orientationally ordered phase; however, a complete understanding of phase III is a work in progress (e.g., Silvera and Dias 2021). In this review, following the classical treatment, phases I, II, and III are described as disordered, partially ordered, and ordered phases, respectively.

Because orientational ordering is more pronounced at low temperatures and under high pressures, we reasoned that low-temperature, high-pressure experiments would be effective in elucidating guest orientational ordering and the corresponding phase transition (Tanaka et al. 2013; Hirai et al. 2012). Helium-refrigerated cryostats installed at SPring-8 (BL10XU) and KEK-PF (BL18C) synchrotron facilities have been used, and pressure control of the sample has been accomplished using a membrane with a gas-driven pressure control system. The pressure and temperature ranges used are 2–77 GPa and 10–300 K, respectively. In addition, the rotational state is influenced by the interaction potentials of local environment, which may be affected by the mass of the host and guest. Even if the ^{1}H and ^{2}H interaction potentials are effectively identical, the rotational state is likely to change if the energy level shifts with mass. For solid hydrogen, phase boundaries among phases I, II, and III considerably differ owing to differences in the mass between D_2 and H_2 (Howie et al. 2012b). The rotational state of HH is similarly expected to change depending on the mass of the guest and host. Therefore, experiments have been conducted in HH samples using H_2 and D_2 as guests and H_2O and D_2O as hosts. In addition, experiments have been conducted in MH samples with H_2O and D_2O as hosts.

4.2 Low-temperature and high-pressure phase transitions of MH

In solid methane, many studies have investigated the progression of molecular orientational ordering and associated phase changes mainly by spectroscopic methods. In the order of increasing pressure, the phases are phase I (disordered phase), phase A (disordered phase), phase B (partially ordered phase), and HP phase (e.g., Bini et al. 1995). The crystal structures of phase I (Hazen et al. 1980), phase A (Nakahata et al. 1999), and phase B (Umemoto et al. 2002) have been reported. Further, Maynard-Casely et al. (2014) determined the carbon substructure of phase B by synchrotron XRD. Recently, the structure of the HP phase has been determined using single-crystal synchrotron XRD and Raman spectroscopy, while first-principles calculations have been used to clarify the position of hydrogen (Bykov et al. 2021). Good agreement was observed between their experimental and calculated Raman vibrational modes, where the changes in the vibrational mode effectively indicated the progression of ordering. They also showed a figure overlaying their Raman data with ours (Hirai et al. 2008b) and that of Chen et al. (2011). Up to ~ 35 GPa, although the resolution of our Raman spectrum was lower than that of Bykov et al., the observed vibration modes for phases A, B, and HP1 were consistent.

For solid methane, the vibrational modes of methane molecules (n_1 and n_3) split during the phase transitions from phase A (disordered state) to phase B (partially ordered state) and further to the HP phase (e.g., Chen et al. 2011; Hirai et al. 2008b). In our experiment involving MH, a similar splitting of the vibrational modes to that observed for the transition from phase A to phase B in solid methane began at 15 GPa and was enhanced with increasing pressure, suggesting that a similar ordering of guest molecules also occurred in MH (Tanaka et al. 2013; Machida et al. 2007). XRD studies show that the change in axial ratio and the decrease in compressibility of the c-axis with increasing pressure becomes clearer under approximately 20 GPa (Tanaka et al. 2013). The c-axis of the MH-III structure is initially the most compressible axis below 20 GPa because of the wide void channels running perpendicular to the c-axis (Hirai et al. 2003). The pressure at which vibrational mode splitting occurs almost coincides with that at which the changes in the axial ratio and compressibility occur. Thus, the change under approximately 20 GPa is interpreted to be induced by the guest orientational ordering of methane molecules, which may be the cause of the observed change in the axial ratio, and the phase is designated as GOS MH-III (called the guest orientationally ordered state by Tanaka et al. (2013)).

After our experiments described above, Schaack et al. (2018) reported the phase change in MH up to 150 GPa by Raman spectroscopy and ab initio simulations, showing a detailed progression of phase change due to guest ordering at approximately 20 GPa. They described that methane molecules rotate freely in the channel of the ice framework and that the gradual orientational ordering of the guest molecules accompanied by a progressive distortion of the molecules below 20 GPa results in a complete locking-in of guests, that is, completely restricted rotational state, under approximately 20 GPa. Finally, as the pressure exceeds 20 GPa, the host–guest system enters a mode of strong coupling, where dynamics of the methane guest and water host are intimately paired. This host–guest system above 20 GPa reasonably explains the axial ratio change and decrease in c-axis compressibility. This theoretical study clearly verifies our experimental results and interpretation.

At a higher pressure of 34 GPa, further changes in the XRD pattern and Raman vibrational mode are observed, corresponding to the transition from MH-III to MH-IV (Kadobayashi et al. 2020a, b, c; Machida et al. 2008, 2010). At ambient temperature, MH-IV is formed at 34 GPa, while at lower temperatures, the transition occurs at 28 GPa. The O–O distance is too long for hydrogen-bond symmetrization to occur in ice (Pruzan 1994). Therefore, MH-IV formation is interpreted to occur via another ordering state instead of via hydrogen-bond symmetrization (Kadobayashi et al. 2020a, b, c). In subsequent studies by Schaack et al. (2019, 2020), they investigated the mechanism of the phase transition from MH-III to MH-IV using ab initio molecular dynamics calculations and stated that the transition involved hydrogen-bond reconstruction and guest reorientation, highlighting the distinct orientational ordering of the two phases. Their studies provided a theoretical rationale for our interpretation of the transition from MH-III to MH-IV, thereby theoretically verifying the stepwise progression of guest ordering in MH. From our experimental results, an outline of the existence region for the three phases of MH for H_2O and D_2O hosts is obtained, namely the known MH-III (guest disordered phase), GOS MH-III (ordered phase), and MH-IV (further ordered phase), under conditions ranging from 2 to 77 GPa and from 30 to 300 K (Tanaka et al. 2013).

4.3 Low-temperature and high-pressure phase transitions of HH

HH exists in three well-known phases. The first phase comprises the clathrate structure sII, which contains four hydrogen molecules in a 16-hedral cage (Mao et al. 2002; Lokshin et al. 2004). The other two are filled-ice structures, namely C1 with a framework of ice II and C2 with a framework of ice Ic (Vos et al. 1993, 1996). The sII structure is only stable at low temperatures, whereas C1 and C2 are stable at ambient temperatures and high pressures, i.e., C1 exists from 0.9 to 2.7 GPa, while C2 exists above 2.7 GPa. Our group has also conducted numerous experiments on the phase transitions of HH at ambient temperature and found that C2 survives to a pressure of at least 90 GPa (Machida et al. 2008). In addition to these three phases, the following phases are known to exist in HH. C0 was first reported by Efimchenko et al. (2010), and Strobel et al. (2011) defined its existence region at low temperatures. Wang et al. (2020) propose a phase diagram for H_2–H_2O, including C0 and C1′, which is a newly found phase. Strobe et al. (2016) determined the structure of C0, a quartz-like ice framework with molecular hydrogen inside. The protons of the host molecule are disordered, and the rotation of the hydrogen guest molecule is disordered. C0 is formed under 400 MPa at room temperature (280 K) with a nominal composition of $H_2O/H_2 = 2{:}1$, indicating that the phase can store large amounts of hydrogen. Furthermore, C0 exists under the thermodynamic conditions of icy bodies. Qian et al. (2014) predicted the existence of a new Ih-C0 phase (similar to C0) and C3 by first-principles calculations. C3 has been demonstrated to be thermodynamically stable above 38 GPa, but this phase has not been reproduced experimentally.

C2 was first reported as a cubic structure because its framework was cubic ice Ic (Vos et al. 1996); subsequently, first-principles calculations predicted that C2 underwent a phase transition from cubic to tetragonal at low temperatures and high pressures (Zhang et al. 2012). Our group experimentally verified the existence of the predicted tetragonal structure in the same year (Hirai et al. 2012) by low-temperature (10–300 K) and high-pressure (5–50 GPa) experiments using samples with D_2O as host and D_2 as guest. Precise XRD experiments revealed a distinct splitting of diffraction lines above 20 GPa, and the XRD pattern identified a tetragonal structure. To investigate the reason for the formation of the tetragonal phase, the vibrational and rotational modes of the hydrogen molecule were measured using Raman spectroscopy at low temperatures. With increasing pressure to 20 GPa, the vibrational modes minimally changed, but the splitting of the roton mode was observed. The roton split suggested that the transition to the tetragonal structure may be induced by guest rotational restricting or orientational ordering similar to that seen in MH, as described above.

Because the orientational ordering of hydrogen molecules occurs in solid hydrogen, reasonably, it can also occur in HH. Zhang et al. (2012) examined phase changes by first-principles calculations up to 80 GPa and showed that orientational ordering occurred at low temperatures and under high pressures in HH filled-ice structures. Strobel et al. (2009) performed a comprehensive Raman study of the guest rotational states in the clathrate structure sII for H_2 and H_2 + THF hydrate and discussed the guest rotational energy levels based on quantum theory and the implications for their splitting. According to their explanation, the rotational degeneracy of H_2 molecules in the clathrate cages is lifted and observed directly as the splitting of the para-H_2 roton band, and the splitting is explained in relation to the orientational dependence of the rotation and the degree of barrier to free rotation in the clathrate structure. Moreover, the interaction potential and, thus, orientational anisotropy vary in large and small cages. When the H_2 occupancy in large cages increases, orientationally dependent rotation is enhanced, and the barrier to free rotation increases. In

filled-ice structures, the interaction potential is even higher than that in clathrate structures because the frequency of the vibrational mode $Q_1(1)$ of the hydrogen molecule in C2 is considerably higher than that of sII (Mao et al. 2002; Hirai et al. 2007; Machida et al. 2010) and even higher than that for the quadruple occupation of the sII 16-hedron (Strobel et al. 2009). Therefore, in filled-ice structures, the rotational barrier is assumed to be essentially higher than that of the clathrate structure. As mentioned above, Zhang et al. (2012) have shown the rotational ordering of hydrogen molecules in a filled-ice structure and argued that the guest hydrogen molecules change symmetry at low temperatures, which explains the observation of tetragonal symmetry at low temperatures. They have also calculated the enthalpies of several candidate structures and proposed $P4_12_12$ as the most feasible candidate, where the hydrogen molecules are orientationally ordered and the molecular axes of the hydrogen molecules extend along the c-axis direction. Thus, our experimental results and interpretation of the occurrence of guest orientational ordering and the resulting tetragonal structures at 20 GPa are theoretically verified.

In our experiments involving HH, three phase transitions were observed in HH filled-ice above C2 (e.g., Machida et al. 2008). The first transition has been verified by Zhang et al. (2012), as described previously. The second and third transitions to HH-HP1 and HH-HP2 structures, respectively, have been observed by the XRD and Raman study. In the second transition to HH-HP1 under approximately 40 GPa, the split in the XRD lines observed is intrinsic and not due to stresses in the sample chamber (Machida et al. 2008). Particularly in low-temperature experiments, this split and its pressure changes are clearly observed, and HH-HP1 is shown to exist under pressures exceeding 40 GPa from ambient temperature to 70 K (Hirai et al. 2012). In addition, a change in the slope of Raman shift of vibrational mode versus pressure is observed under 38–40 GPa, and a notable decrease in the intensity of the roton mode is observed under 40 GPa (Machida et al. 2010). This phase has been observed with good reproducibility in our experiments (Machida et al. 2008, 2010; Hirai et al. 2012). The findings suggest that another orientationally ordered structure or further rotation-restricted state may be formed. Considering the stepwise progression of ordering occurring in MH, solid hydrogen, and methane, it could be inferred that stepwise ordered states may develop in HH. The elucidation of the detailed structures of the phase is a future research direction. In the third transition to HH-HP2 under approximately 60 GPa, the splitting of diffraction lines (Machida et al. 2008; Hirai et al. 2012) and change in vibration mode in Raman spectra are clearly observed (Machida et al. 2010). However, whether this phase is a phase with further orientational ordering or one related to hydrogen-bond symmetrization is currently unknown.

Based on the experimental results, the existence regions for three phases, C2, tetragonal phase, and HH-HP1, have been proposed in the ranges of 5–50 GPa and 10–300 K (Hirai et al. 2012). Solid hydrogen has three phases (I, II, and III) with different degrees of ordering at low temperatures. To reach phase III, that is, the classically ordered phase, a high pressure of 160 GPa is required (e.g., Hemley and Mao 1996). By contrast, HH requires a pressure of only 40 or 60 GPa to achieve the highly restricted rotational state. This suggests the existence of an enhanced interaction potential in the host framework of HH that strongly affects guest rotation.

During experimental and theoretical studies on solid hydrogen under a wide range of conditions, five solid phases and their sub-phases have been reported, and their structures have been discussed in detail. For example, the structure of phase IV has been under debate (e.g., Howie et al. 2012a, b; Ackland and Loveday 2020; Magdău and Ackland 2013). Certain challenges have also been encountered in verifying solid metallic hydrogen (e.g., Eremets et al. 2019; Zha et al. 2012; Goncharov and Struzhkin 2017). Furthermore, the plasma phase boundary in hot dense liquid hydrogen has been discussed (Morales et al. 2010; Ohta et al. 2015). Silvera and Dias (2021) have provided an overview of the research that has been conducted since the metallization of hydrogen was first reported by Wigner and Huntington (1935).

5 Pressure-dependent structural evolution

The interpretation of our experimental results on MH has been theoretically verified. For HH, the first ordering step inducing tetragonal structure has also been verified, but HH-HP1 and HH-HP2 have yet to be verified to date. However, based on the similarities to MH and solid hydrogen, similar ordering progression and structural changes in HH seem reasonable. Considering these points, an overview of the structural changes specific to guest–host structures can be inferred. Figure 4 shows a schematic diagram of the phase transitions induced by guest orientational ordering and those caused by host hydrogen-bond symmetrization after transition to the filled-ice structure for MH and HH. For MH, orientational ordering of the guest starts under approximately 15 GPa, inducing a change in the axial ratio of the same orthorhombic structure (guest-ordered MH-III). Under 34 GPa, another orientational ordering step occurs, resulting in the change of the structure to MH-IV. Additionally, theoretical calculations have predicted that host hydrogen-bond symmetrization occurs at higher pressure (Iitaka and Ebisuzaki 2003;

Schaack et al. 2019). For HH, the quartz-like structure C0 changes to the filled-ice structure C1 under 0.7 GPa, C1 changes to C2 under 2.7 GPa, and C2 is maintained up to approximately 20 GPa, under which pressure the guest undergoes orientational ordering, thus inducing a tetragonal guest-ordered C2 (Hirai et al. 2012; Zhang et al. 2012). Under ~ 40 GPa, another phase change to HH-HP1 occurs, which is probably induced by further orientational ordering. For HH, a theoretical study relating to symmetrization has not been reported, but Lei et al. (2021) conducted an experiment with the H_2–H_2O and He–H_2O systems up to 130 GPa, using H_2 and He as the pressure media. Well-resolved XRD has revealed that a transition from ice VII to ice X, i.e., hydrogen-bond symmetrization, occurs under 20–50 GPa in the H_2–H_2O system. When H_2 is incorporated into ice VII, HH-C2 may be formed under pressures exceeding 2.7 GPa. However, the details of the phase formed in that experiment remain unclear.

In general, MH and HH behave similarly under high pressure, both involving guest stepwise ordering and host hydrogen-bond symmetrization. However, the individual phase transitions of MH and HH exhibit distinct behaviors owing to differences in the initial filled-ice host structure and in the properties of the guest molecules. Regarding the relationship between molecular symmetry lowering or distortion and induced structural changes, Ackland and Loveday (2020) examined solid hydrogen phase I and found that the change in the axial ratio, c/a, was correlated to the change in cos θ (where θ is the angle between the molecular axis and the c-axis of the hcp crystal). They demonstrated that the molecules in phase I started to rotate in the basal plane and the molecular symmetry lowered from spherical to toroidal; in addition, a transition to a toroidal molecular symmetry did not lead to a structural change when the symmetry was compatible with the $P6_3/mmc$ of the phase I structure. For MH, a theoretical analysis by Schaack et al. (2018) showed that under 20 GPa, the guest was completely fixed and distorted. The molecular distortion and ordering at this step appeared as an axial ratio change within the same structure of MH-III without any structural change (Tanaka et al. 2013). Subsequently, under 40 GPa, further reordering of the guest occurred, causing a structural change to another orthorhombic structure (MH-IV) (Schaack et al. 2019; Kadobayashi et al. 2020a, b, c). For HH, the guest hydrogen molecular axis was oriented in the c-axis direction of the structure, leading to a structural change to a tetragon because the initial structure was cubic (Zhang et al. 2012; Hirai et al. 2012). Thus, the structural changes induced by ordering in both hydrates proceed via different ways depending on the initial framework structure and degree of ordering.

Clathrate structures recombine their cages in response to pressure; when they can no longer maintain the cage structure, they successfully reorganize into a unique filled-ice structure and undergo several further phase transitions. Particularly for MH and HH, such phase transitions enable their stability up to ultrahigh pressures (above 100 GPa). In Sect. 2, we noted that the outstanding high-pressure stability of MH and HH is most likely due to guest–host interactions. In our series of studies, we have explored the origins of the distinctive stability of these two hydrates and found that the freely rotating guest molecules at low pressures and ambient temperatures undergo orientational ordering with increasing pressure and decreasing temperature. This ordering proceeds in a stepwise manner, causing sequential structural changes toward phases that are more stable under high pressures. Furthermore, even under elevated pressures, hydrogen-bond symmetrization of the host water molecule has been predicted, which can further enhance the stability. Thus, hydrates respond to external pressure changes via a common process, such as stepwise guest orientational ordering and host hydrogen-bond symmetrization, to achieve self-organization. In biological evolution, organisms adapt to changes in the environment and evolve accordingly, that is, promote self-organization, by modifying their form and function. When looking at hydrates from this point of view, structural changes can be viewed as "structural evolution" in response to changes in pressure by creating a function of guest ordering and host-bond symmetrization. The common evolutional process for MH and HH hydrates has not yet been fully established either experimentally or theoretically, but we have proposed such a perspective on the phase change of hydrates composed of multi-component host–guest systems (Hirai and Kadobayashi 2018; Kadobayashi et al. 2020a).

6 High-temperature and high-pressure properties

6.1 Does MH melt, decompose, or change phases?

We have discussed the physical properties of hydrates under high pressures at ambient and low temperatures in the preceding sections. This section discusses the physical properties of hydrates under both high-temperature and high-pressure conditions. Experiments at mildly elevated temperatures and pressures have provided insight into the origin of methane in the Earth's upper mantle (Kolesnikov et al. 2009). Petroleum is known to originate from a biological process; however, experiments on the polymerization of solid methane under moderately high pressures and at high temperatures indicate that hydrocarbons in the upper mantle may have been produced by abiogenic processes (Kolesnikov et al. 2009). This implies the role of solid methane in geochemically

important processes. Relatively few studies have been conducted on the high-temperature and high-pressure properties of gas hydrates (Kurnosov et al. 2001; Bezacier et al. 2014). However, MH and HH are thought to be widespread in the solar system and beyond, such as in protostars and icy bodies, where hydrates are likely to be exposed to a wide range of temperature and pressure conditions (e.g., Marboeuf et al. 2010). Various temperature and pressure conditions inside icy bodies have been reported. For Titan, the ice mantle-to-core conditions are estimated to be 0.55–6 GPa and 270–1000 K (Grasset et al. 2000; Tobie et al. 2005). We have shown that MH can thermodynamically exist in the upper layers of the Titan ice mantle by experiments under temperature and pressure conditions comparable to those in the interior of Titan and through internal structure models (Kadobayashi et al. 2020b), and Loveday et al. (2001a, b) have reported similar results. The source of the methane-rich atmosphere of Titan has been discussed, and thermal cycling, cryovolcanism (e.g., Choukroun et al. 2010), and other processes have been proposed. The mechanism of supplying methane to the atmosphere has not yet been clarified, but MH present in the ice mantle is considered to be the most likely source (Loveday et al. 2001a; Bezacier et al. 2014). The conditions in the uppermost part of Neptune's ice mantle are estimated to be 10 GPa with a temperature of 2200 K (Nettelmann et al. 2016). The existence of a high-pressure MH phase and a novel high-pressure phase in the C–H–O system are intriguing options. We conducted high-temperature and high-pressure experiments (2–55 GPa and 298–653 K) using an externally heated DAC equipped with a band heater to elucidate whether MH-III and MH-IV melt or decompose into solid methane and high-pressure ice (Kadobayashi et al. 2018, 2020b, c). The bulk composition of the sample used in these experiments was estimated to be $H_2O/CH_4 = 2{:}1$.

6.2 Stability region and dissociation curve of MH-III and MH-IV

All sequential in situ Raman spectroscopy measurements have revealed that MH-III melts into liquid water and liquid methane under pressures below ~ 2.5 GPa and decomposes into solid methane and ice VII above ~ 2.5 GPa, i.e., solid–solid phase decomposition (Kadobayashi et al. 2018, 2020b, c). Dyadin et al. (1997) performed the first high-pressure experiments to determine the melting curve of MH-I and MH-II below 1.5 GPa, and the results of our melting experiments on MH-I and MH-II in the H_2O–CH_4 system are in good agreement with theirs. Our studies on the H_2O–CH_4–NH_3 system also confirmed that the melting curves of MH-I and MH-II are higher than those of ice (Kadobayashi et al. 2020b), as shown by Dyadin et al. (1997). By contrast, MH-III and MH-IV decompose into solid methane and ice VII in the pressure region of this experiment (Fig. 5) (Kadobayashi et al. 2018). In addition to sequential Raman spectroscopy, XRD studies were conducted to analyze samples heated to temperatures above and below the obtained dissociation curve, thus confirming the existence of solid methane and ice VII at higher temperatures and of MH-III or MH-IV at lower temperatures (Kadobayashi et al. 2018). The obtained dissociation curve is approximately 200 K lower than those for ice VII and solid methane (Lin et al. 2005; Lobanov et al. 2013). Our experimental results deviate from those of the previous two experiments by Kurnosov et al. (2001) and Bezacier et al. (2014). This difference can be attributed to the different systems used in the experiments: A system including ammonia has been utilized in one previous experiment (Kurnosov et al. 2001), while the other experiment has insufficiently determined the start of melting (Bezacier et al. 2014). The melting of MH-I and MH-II below ~ 2.5 GPa can be easily seen by optical observation. Meanwhile, the solid–solid decomposition of MH-III and MH-IV under pressures exceeding ~ 2.5 GPa does not exhibit visible differences in appearance before and after decomposition; therefore, the decomposition should be determined based on continuous measurements by in situ Raman spectroscopy and XRD, as conducted in our experiments (Kadobayashi et al. 2018). By contrast, Bezacier et al. (2014) declared their use of Raman spectroscopy and optical observation for determining decomposition, but they did not compare the Raman spectra during MH dissociation. This suggests that Bezacier et al. determined the decomposition conditions of MH-III mainly based on optical observations, which is similar to their approach used for investigating the melting of MH-I and MH-II. In our experiments, the samples that have been observed to decompose into solid methane and ice VII by sequential Raman measurements melt at higher temperatures than that of the decomposition, i.e., near the melting curve of ice VII. This outcome shows significant changes in their appearance, which is similar to the melting behavior of MH-I and MH-II. Therefore, visual observation alone is not sufficient to determine the decomposition conditions of MH-III and MH-IV. The different methods used to determine decomposition have apparently resulted in a significant difference in the decomposition curves (Kadobayashi et al. 2018, 2020b, c).

The results discussed thus far demonstrate that MH-IV is stable up to 633 K under a pressure of 40.3 GPa, suggesting the possible presence of high-pressure phases of MH in icy bodies and newly discovered exoplanets (cool planets with relatively low internal temperatures). Meanwhile, MH cannot exist in the icy mantle of Neptune and

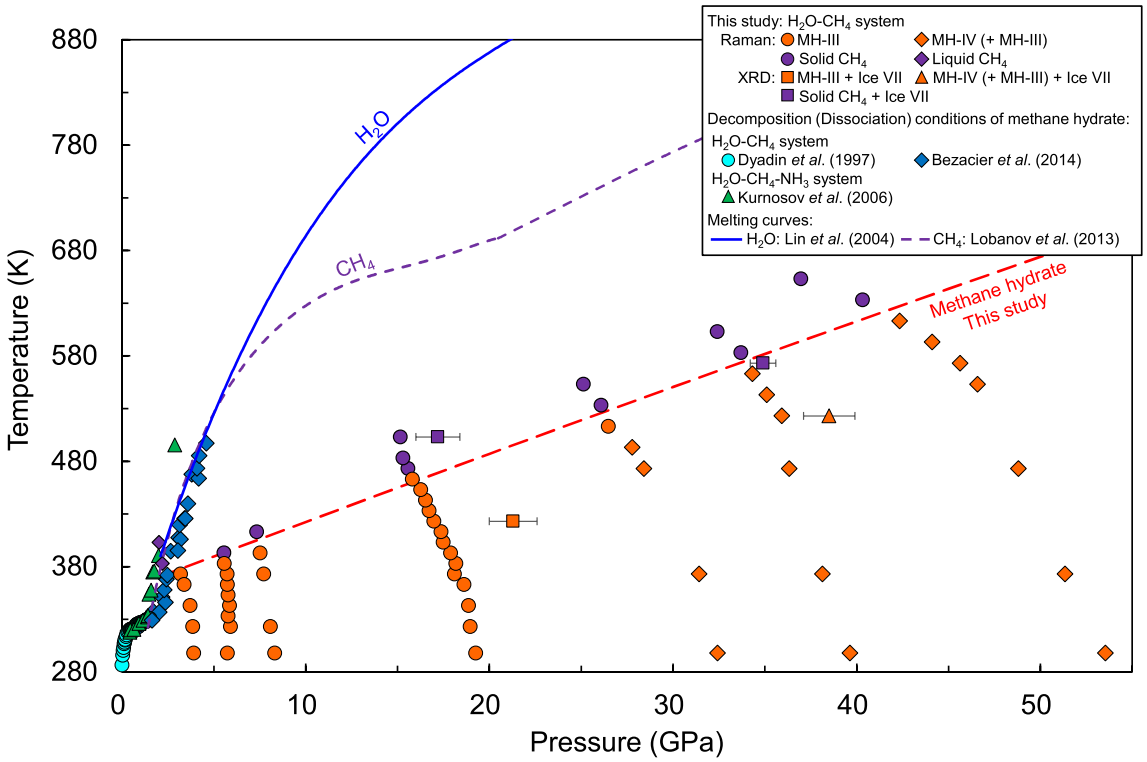

Fig. 5 Stability region of MH-III and MH-IV based on sequential Raman spectra. MH-III melts below 2.5 GPa and decomposes into solid methane and ice VII above 2.5 GPa. MH-IV exhibits solid decomposition. The broken line indicates the obtained dissociation curve. The dissociation curve is approximately 200 K lower than the melting curves of solid methane and ice VII. This figure is modified from Kadobayashi et al. (2018)

Uranus because of the high-temperature conditions in these planets.

6.3 Significance of MH stability in planetary science

MH-III and MH-IV decompose into solid methane and ice VII under the conditions shown in Fig. 5, and solid methane and ice VII melt according to their own melting curves at elevated temperatures (Lin et al. 2005; Lobanov et al. 2013). To determine the effect of higher temperatures, our group has conducted high-temperature and high-pressure experiments using a laser-heated DAC (Kadobayashi et al. 2021). Solid methane has been subjected to numerous experiments and theoretical calculations by our group and others, and the molecular dissociation of methane molecules and subsequent diamond formation have been reported (e.g., Gao et al. 2010; Hirai et al. 2008b, 2009; Benedetti et al. 1999; Ancilotto et al. 1997). In most previous experiments, metal has been added to the sample chamber as a laser absorber, and its effect on the phase change and diamond formation can be considered to be non-negligible. Several shock-compression experiments have also been reported, but the dynamic compression and shock duration in these experiments are not comparable to those estimated in the interior of planets (Nettelmann et al. 2016).

To investigate the intrinsic behavior of MH, we conducted experiments on the methane–water system using a CO_2 laser for heating (Kadobayashi et al. 2021) to avoid the need for metallic absorbers. These experiments were designed to analyze the MH sample alone under static compression conditions closer to those estimated for Neptune's upper mantle (Nettelmann et al. 2016), i.e., 45 GPa and up to 3800 K. Consequently, both solid methane and ice melted, methane molecules underwent molecular dissociation, and diamonds were formed from carbon, as detected by in situ XRD. Moreover, octahedral-shaped diamond particles were observed in the recovered sample quenched under ambient temperature and pressure conditions, and Raman spectroscopy revealed a characteristic Raman peak for the diamonds at 1331 cm^{-1}. The presence of hydrogen molecules was also observed in the sample chamber (Kadobayashi et al. 2021). Although several experimental reports on diamond formation have been published (e.g., Zerr et al. 2006; Kraus et al. 2017), our in situ XRD, Raman spectroscopy, and SEM observations and recovered sample data provide unambiguous evidence for diamond

formation based on theoretical prediction made 40 years ago (Ross 1981). In addition, our results demonstrate that when discussing the phase evolution of the water–methane system under high-temperature and high-pressure conditions, the C–H–O system should be discussed rather than the bimolecular H_2O–CH_4 system.

As shown in Fig. 6, the diamond formation observed in our experiments (Kadobayashi et al. 2021) occurred under milder conditions than those previously reported. Wentorf (1965) reported that the conditions of diamond formation depend significantly on the composition of the initial hydrocarbon material. The MH sample that we used as a starting material contained a large amount of water. A theoretical study on the role of water reported that ionized water under high-temperature and high-pressure conditions acts as an exceptionally aggressive chemical solvent and dissociates methane (Lee and Scandolo 2011). The mild conditions we observed for diamond formation may be due to the influence of water. In addition, the analysis timescale depends on the experimental method: picoseconds for atomic simulations, nanoseconds for dynamic laser compression experiments, and seconds to minutes for laser-heated DAC experiments. Therefore, the timescales of the atomic simulations and dynamic laser compression experiments may be too short to observe diamond formation from hydrocarbon materials, and thus, higher pressures and temperatures are required.

Neptune is believed to have a hydrogen and helium atmosphere; an ice mantle containing water, methane, and ammonia; and a rocky core (Redmer et al. 2011; Nettelmann et al. 2013). The findings of our experiments (Kadobayashi et al. 2021; Kadobayashi et al. 2020a, b, c) indicate that diamonds are formed by the molecular dissociation and polymerization of methane molecules in the presence of water at significantly lower temperatures and pressures ($T > 1600$ K, $P > 13$ GPa) than previously reported. The temperature and pressure conditions for diamond formation overlap with the predicted internal conditions of icy planets (Nettelmann et al. 2016), demonstrating that diamond formation can occur in the upper regions of the ice mantle of an icy planet.

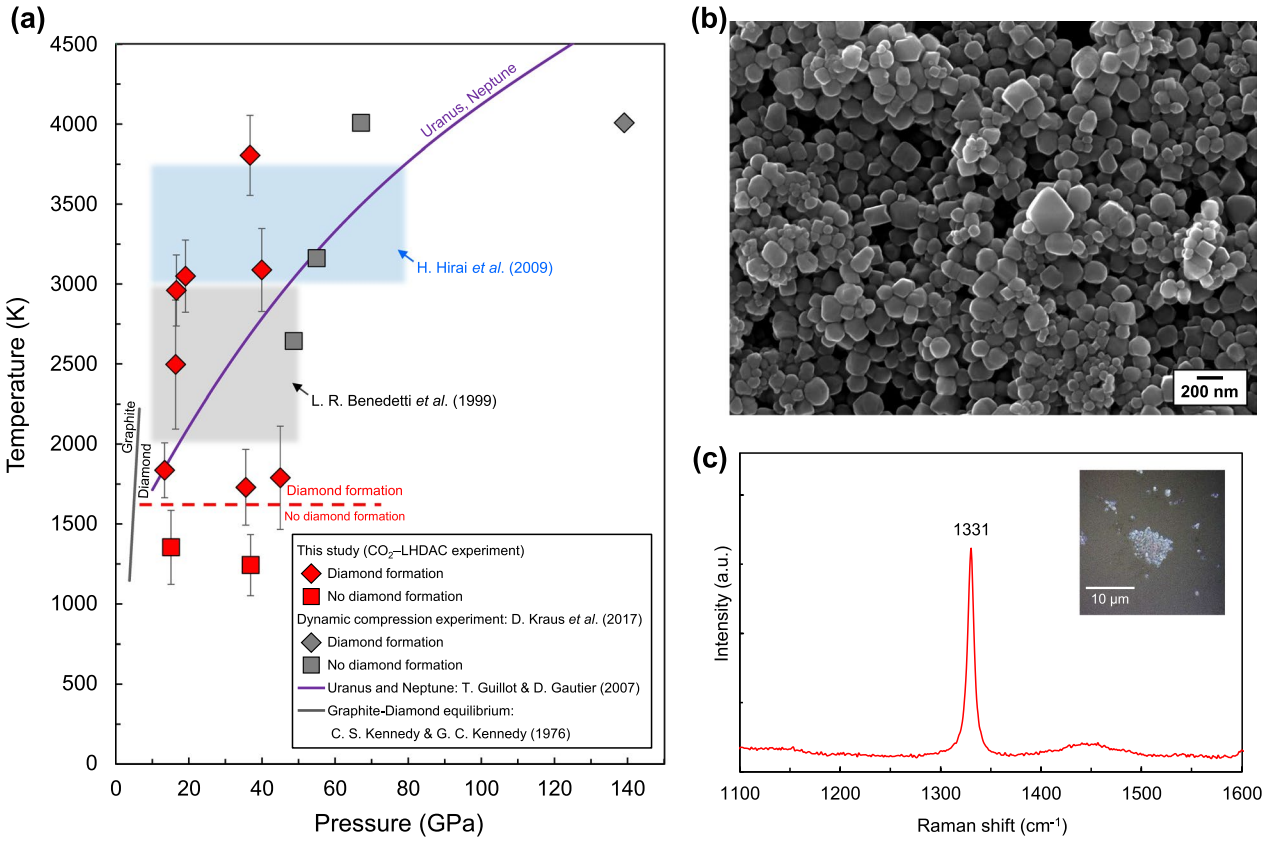

Fig. 6 Diamond formation by melting and the molecular dissociation of methane at extremely high temperatures and pressures. **a** Region of diamond formation. **b** SEM image of diamond particles recovered at ambient temperature and pressure, including octahedral particles. **c** Raman spectra of the recovered sample on a glass slide with the characteristic peak for diamond at 1331 cm^{-1}. This figure is modified from Kadobayashi et al. (2021)

Because diamonds have a higher density than the surrounding icy material, they may settle toward the core of the icy planet, forming a layer of diamonds around the rocky core. Diamond formation and deposition in the interiors of these icy planets not only constrain the modeling of their internal structure but also provide clues for understanding their characteristic heat budget and magnetic field. For example, Neptune emits more energy than it receives from the sun. The source of this excess heat has long remained a mystery, but it has been suggested to originate from the frictional heat generated by diamonds settling within the surrounding icy material (Naumova et al. 2021; Kraus 2018). Additionally, if hydrogen, a by-product of diamond formation, is metalized under extreme pressures deep within the planet (e.g., Li et al. 2021), it may contribute to the magnetic fields of Uranus and Neptune as a conductor, along with the superionic phases of water and ammonia (Kraus 2018).

7 Conclusions

The high-pressure properties of clathrates and filled-ice hydrates are gradually being elucidated. However, several issues require further research focus, such as clarification of the detailed structure of the guest orientationally ordered phases, experimental verification of hydrogen-bond symmetrization at high pressures, proton ordering at low temperatures, and the physical properties of the C–H–O system at extremely high temperatures and pressures. Exploring unknown phases and their physical properties under a range of conditions is critical for planetary science because they provide data for modeling studies on the formation and evolution of icy bodies in space. Given the broad range of temperature and pressure conditions in the universe, ice and hydrates are expected to undergo a diverse structural evolution and develop novel physical properties. Accordingly, such systems offer immense scope for novel discoveries. The continual progression of this research field is expected to shed further light on these intriguing materials and their role in the universe.

Acknowledgements
We would like to express our gratitude to Professor Emeritus Eiji Otani, former General Editor, for giving us the opportunity to write this review. We also thank Professor Shoichi Yoshioka, Editor-in-Chief of Section Science, and Dr. Bjorn Mysen, Editor, for their constructive suggestions. We are grateful to Dr. Yoshitaka Yamamoto and Dr. Satoshi Takeya, National Institute of Advanced Industrial Science and Technology, for their valuable comments.

Author contributions
HH conceived and designed this review. HH and HK collected and arranged previous studies. HH wrote and revised the manuscript. HH and KH equally contributed to this review, and both have been designated as corresponding authors. Both authors read and approved the final manuscript.

Funding
This study was supported by the Grant-in-Aid for Scientific Research Nos. 22244055, 19656251, 19GS02050015, 18340126, 14550871, 12650915, 08454229, 07213208, and 06640612 to HH and Nos. 17J05467, 19J01467, 19K14815, and 22K14127 to HK from the Japan Society for the Promotion of Science (JSPS).

Availability of data and materials
Representative data such as X-ray diffractometry and Raman spectroscopy supporting the conclusions of this article are included within the cited articles in the text.

Declarations

Competing interests
The authors declare that they have no competing interests.

Received: 16 May 2022 Accepted: 5 January 2023
Published online: 13 January 2023

References

Ackland GJ, Loveday JS (2020) Structures of solid hydrogen at 300 K. Phys Rev B 101:094104. https://doi.org/10.1103/PhysRevB.101.094104
Akahama Y, Nishimura M, Kawamura H, Hirao N, Ohishi Y, Takemura K (2010) Evidence from x-ray diffraction of orientational ordering in phase III of solid hydrogen. Phys Rev B 82:060101. https://doi.org/10.1103/PhysRevB.82.060101
Alavi S, Dornan P, Woo TK (2008) Determination of NMR lineshape anisotropy of guest molecules within inclusion complexes from molecular dynamics simulations. Chem Phys Chem 9:911–919. https://doi.org/10.1002/cphc.200700805
Alavi S, Susilo R, Ripmeester JA (2009) Linking microscopic guest properties to macroscopic observables in clathrate hydrates: guest–host hydrogen bonding. J Chem Phys 130:174501. https://doi.org/10.1063/1.3124187
Ancilotto F, Chiarotti GL, Scandolo S, Tosatti E (1997) Dissociation of methane into hydrocarbons at extreme (planetary) pressure and temperature. Science 275:1288–1290. https://doi.org/10.1126/science.275.5304.1288
Aoki K, Yamawaki H, Sakashita M, Fujihisa H (1996) Infrared absorption study of the hydrogen-bond symmetrization in ice to 110 GPa. Phys Rev B 54:15673–15677. https://doi.org/10.1103/PhysRevB.54.15673
Benedetti LR, Nguyen JH, Caldwell WA, Liu H, Kruger M, Jeanloz R (1999) Dissociation of CH4 at high pressures and temperatures: diamond formation in giant planet interiors? Science 286:100–102. https://doi.org/10.1126/science.286.5437.100
Bezacier L, Menn E, Grasset O, Bollengier O, Oancea A, Mezouar M, Tobie G (2014) Experimental investigation of methane hydrates dissociation up to 5 GPa: implications for Titan's interior. Phys Earth Planet Inter 229:144–152. https://doi.org/10.1016/j.pepi.2014.02.001
Bini R, Pratesi G (1997) High-pressure infrared study of solid methane: phase diagram up to 30 GPa. Phys Rev B 55:14800. https://doi.org/10.1103/PhysRevB.55.14800
Bini R, Ulivi L, Jodl HJ, Salvi PR (1995) High pressure crystal phases of solid CH4 probed by Fourier transform infrared spectroscopy. J Chem Phys 103:1353. https://doi.org/10.1063/1.469810
Burger BJ, Estrada MV, Gustin MS (2019) What caused Earth's largest mass extinction event? New evidence from the Permian-Triassic boundary in northeastern Utah. Glob Planet Change 177:81. https://doi.org/10.1016/j.gloplacha.2019.03.013
Bykov M, Bykova E, Pickard CJ, Martinez-Canales M, Glazyrin K, Smith JS, Goncharov AF (2021) Structural and vibrational properties of methane up to 71 GPa. Phys Rev B 104:184105. https://doi.org/10.1103/PhysRevB.104.184105
Cha M, Shin K, Lee H, Moudrakovski IL, Ripmeester JA, Seo Y (2015) Kinetics of methane hydrate replacement with carbon dioxide and nitrogen gas mixture using in situ NMR spectroscopy. Environ Sci Technol 49:1964–1971. https://doi.org/10.1021/es504888n

Chen JY, Yoo CS (2012) Formation and phase transitions of methane hydrates under dynamic loadings: compression rate dependent kinetics. J Chem Phys 136:114513. https://doi.org/10.1063/1.3695212
Chen PN, Zha CS, Chen XJ, Shu J, Hemley RJ, Mao HK (2011) Raman study of phase transitions in compressed methane using moissanite anvil cells. Phys Rev B 84:104110. https://doi.org/10.1103/PhysRevB.84.104110
Chou I-M, Sharma A, Burruss RC, Shu J, Mao H-K, Hemley RJ, Goncharov AF, Stern LA, Kirby SH (2000) Transformations in methane hydrates. Proc Natl Acad Sci USA 97:13484. https://doi.org/10.1073/pnas.250466497
Choukroun M, Grasset O, Tobie G, Sotin C (2010) Stability of methane clathrate hydrates under pressure: influence on outgassing processes of methane on Titan. Icarus 205:581–593. https://doi.org/10.1016/j.icarus.2009.08.011
Davidson DW (1973) Clathrate hydrates. In: Franks F (eds) Water in crystalline hydrates aqueous solutions of simple nonelectrolytes. Water, Vol 2. Chapt.3. Springer, Boston, MA. https://doi.org/10.1007/978-1-4757-6958-6_3
Davidson DW, Leaist DG, Hesse R (1983) Oxygen-18 enrichment in the water of a clathrate hydrate. Geochim Cosmochim Acta 47:2293–3229. https://doi.org/10.1016/0016-7037(83)90053-4
Davidson DW, Garg SK, Gough SR, Handa YP, Ratcliffe CL, Tse JS, Ripmeester JA (1984a) Some structural and thermodynamic studies of clathrate hydrates. J Inclusion Phenom 2:231–238. https://doi.org/10.1007/BF00663261
Davidson DW, Handa YP, Ratcliffe CI, Tse JS, Powell BM (1984b) The ability of small molecules to form clathrate hydrates of structure II. Nature 311:142–143. https://doi.org/10.1038/311142a0
Davidson DW, Handa YP, Ripmeester JA (1986) Xenon-129 NMR and the thermodynamic parameters of xenon hydrate. J Phys Chem 90(24):6549–6552. https://doi.org/10.1021/j100282a026
Davies SR, Sloan ED, Sum AK, Koh CA (2010) In situ studies of the mass transfer mechanism across a methane hydrate film using high-resolution confocal Raman spectroscopy. J Phys Chem C 114:1173–1180. https://doi.org/10.1021/jp909416y
Deng Y, Chen F, Guo Q, Hu Y, Chen D, Yang S, Cao J, Chen H, Wei R, Cheng S, Zhou J, Liu C, Iang X, Zhu J (2021) Possible links between methane seepages and glacial-interglacial transitions in the South China sea. Geophys Res Lett 48:e2020GL091429. https://doi.org/10.1029/2020GL091429
Dyadin YA, Aladko EY, Udachin KA, Tkacz M (1994) The solubility of helium and hydrogen in ice Ih at high pressures. Polish J Chem 68:343–348
Dyadin YA, Aladko EY, Larionov EG (1997) Decomposition of methane hydrates up to 15 kbar. Mendeleev Commun 7:34–35. https://doi.org/10.1070/MC1997v007n01ABEH000655
Dyadin YA, Larionov EG, Manakov AY, Zhurko FV, Aladko EY, Mikina TV, Komarov VY (1999) Clathrate hydrates of hydrogen and neon. Mendeleev Commun 9:209–210. https://doi.org/10.1070/MC1999v009n05ABEH001104
Efimchenko VS, Kuzovnikov MA, Fedotov V, Sakharov M (2010) New phase in the water–hydrogen system. J Alloys Compd 509:S860–S863. https://doi.org/10.1016/j.jallcom.2010.12.200
Eremets MI, Drozdov AP, Kong PP, Wang H (2019) Semimetallic molecular hydrogen at pressure above 350 GPa. Nat Phys 15:1246–1249. https://doi.org/10.1038/s41567-019-0646-x
Franks F, Reid DS (1973) Water: a comprehensive treatise. In: Franks F (ed) 2 *1, Chapter 5. Plenum Press, New York (1973)
Gao G, Oganov AR, Ma Y, Wang H, Li P, Li Y, Iitaka T, Zou G (2010) Dissociation of methane under high pressure. J Chem Phys 133:144508. https://doi.org/10.1063/1.3488102
Goncharov AF, Struzhkin VV (2017) Comment on "Observation of the Wigner-Huntington transition to metallic hydrogen." Science 357:715. https://doi.org/10.1126/science.aam9736
Goncharov AF, Struzhkin VV, Somayazulu M, Hemley RJ, Mao HK (1996) Compression of ice to 210 GPa: evidence for a symmetric hydrogen bonded phase. Science 273:218–220. https://doi.org/10.1126/science.273.5272.218
Grasset O, Sotin C, Deschamps F (2000) On the internal structure and dynamics of Titan. Planet Space Sci 48:617. https://doi.org/10.1016/S0032-0633(00)00039-8
Hanfland M, Hemley RJ, Mao HK (1993) Novel infrared vibron absorption in solid hydrogen at megabar pressures. Phys Rev Lett 70:3760. https://doi.org/10.1103/PhysRevLett.70.3760
Hazen RM, Mao HK, Finger LW, Bell PM (1980) Structure and compression of crystalline methane at high pressure and room temperature. Appl Phys Lett 37:288. https://doi.org/10.1063/1.91909
Hemley RJ (2010) Percy W. Bridgman's second century. High Press Res 30:581–619. https://doi.org/10.1080/08957959.2010.538974
Hemley RJ, Mao HK (1996) Dense molecular hydrogen: order, disorder, and localization. J Non-Cryst Solids 205–207:282–289. https://doi.org/10.1016/S0022-3093(96)00238-4
Hirai H (2009) From carbon materials to gas hydrates: high-pressure properties of gas hydrates and solid methane in the icy planets and their moon—2008 Award winners and their studies. Jpn Mag Miner Petrol Sci 38:1–8. https://doi.org/10.2465/gkk.38.1. (**in Japanese with English abstract**)
Hirai H, Kadobayashi H (2018) Properties of gas hydrates under low to high temperatures and high pressures and their implications of interiors of icy bodies. J Crystallogr Soc Japan 60:54–61. https://doi.org/10.5940/jcrsj.60.54. (**in Japanese with English abstract**)
Hirai H, Uchihara Y, Fujihisa H, Sakashita M, Katoh E, Aoki K, Nagashima K, Yamamoto Y, Yagi T (2001) High-pressure structures of methane hydrate observed up to 8 GPa. J Chem Phys 115:7066–7070. https://doi.org/10.1063/1.1403690
Hirai H, Uchihara Y, Nishimura Y, Kawamura T, Yamamoto Y, Yagi T (2002a) Structural changes of argon Hydrate under high pessure. J Phys Chem B 106:11089–11092. https://doi.org/10.1021/jp021458l
Hirai H, Uchihara Y, Kawamua T, Yamamoto Y, Yagi T (2002b) Pressure-indued phase changes of argon hydrate and methane hydrate at room temperature. Proc Jpn Acad Ser B 78:39–44. https://doi.org/10.2183/pjab.78.39
Hirai H, Tanaka T, Kawamura T, Yamamoto Y, Yagi T (2003) Retention of filled ice structure of methane hydrate up to 42 GPa. Phys Rev B 68:172102. https://doi.org/10.1103/PhysRevB.68.172102
Hirai H, Tanaka T, Kawamura T, Yamamoto Y, Yagi T (2004) Structural changes in gas hydrates and existence of a filled ice structure of methane hydrate above 40 GPa. J Phys Chem Solid 65:1555–1559. https://doi.org/10.1016/j.jpcs.2003.12.018
Hirai H, Machida S, Kawamura T, Yamamoto Y, Yagi T (2006) Stabilizing of methane hydrate and transition to a new high-pressure structure at 40 GPa. Am Mineral 91:826–830. https://doi.org/10.2138/am.2006.1991
Hirai H, Ohno S, Kawamura T, Yamamoto Y, Yagi T (2007) Changes in vibration modes of hydrogen and water molecules and in lattice parameters with pressure for filled-ice hydrogen hydrates. J Phys Chem C 111:312–315. https://doi.org/10.1021/jp064281u
Hirai H, Konagai K, Kawamura T, Yamamoto Y, Yagi T (2008b) Phase changes of solid methane under high pressure up to 86 GPa at room temperature. Chem Phys Lett 454:212–217. https://doi.org/10.1016/j.cplett.2008.01.082
Hirai H, Takahara N, Kawamura T, Yamamoto Y, Yagi T (2008a) Structural changes and preferential cage occupancy of ethane hydrate and methane-ethane mixed gas hydrate under very high pressure. J Chem Phys 129:224503. https://doi.org/10.1063/1.3036006
Hirai H, Konagai K, Kawamura T, Yamamoto Y, Yagi T (2009) Polymerization and diamond formation from melting methane and their implications in ice layer of giant planets. Phys Earth Planet Inter 174:242–246. https://doi.org/10.1016/j.pepi.2008.06.011
Hirai H, Komatsu K, Honda M, Kawamura T, Yamamoto Y, Yagi T (2010) Phase changes of CO2 hydrate under high pressure and low temperature. J Chem Phys 133:124511. https://doi.org/10.1063/1.3493452
Hirai H, Kagawa S, Tanaka T, Matsuoka T, Yagi T (2012) Structural changes of filled ice Ic hydrogen hydrate under low temperatures and high pressures from 5 to 50 GPa. J Chem Phys 137:074505. https://doi.org/10.1063/1.4746017
Hirai H, Tanaka T, Kagawa S, Matsuoka T, Ohishi Y, Hirao N, Yagi T, Ohtake M, Yamamoto Y (2014) Phase changes Induced by guest orientational ordering on methane and hydrogen hydrates under low temperatures and high pressures. Rev High Press Sci Technol 24:278–287. https://doi.org/10.4131/jshpreview.24.278. (**in Japanese with English abstract**)
Hirai H, Kadobayashi H, Hirao N, Ohishi Y, Ohtake M, Yamamoto Y, Nakano S (2015) Time-resolved x-ray diffraction and Raman studies of the phase

transition mechanisms of methane hydrate. J Chem Phys 142:024707. https://doi.org/10.1063/1.4905482
Howie RT, Guillaume CL, Scheler T, Goncharov AF, Gregoryanz E (2012a) Mixed molecular and atomic phase of dense hydrogen. Phys Rev Lett 108:125501. https://doi.org/10.1103/PhysRevLett.108.125501
Howie RT, Scheler T, Guillaume CL, Eugene Gregoryanz E (2012b) Proton tunneling in phase IV of hydrogen and deuterium. Phys Rev B 86:214104. https://doi.org/10.1103/PhysRevB.86.214104
Iitaka T, Ebisuzaki T (2003) Methane hydrate under high pressure. Phys Rev B 68:172105. https://doi.org/10.1103/PhysRevB.68.172105
Ikeda T, Terakura K (2003) Structural transformation of methane hydrate from cage clathrate to filled ice. J Chem Phys 119:6784. https://doi.org/10.1063/1.1606437
Ikeda T, Yamamuro O, Matsuo T, Mori K, Torii S, Kamiyama T, Izumi F, Ikeda S, Mae S (1999) Neutron diffraction study of carbon dioxide clathrate hydrate. J Phys Chem Solids 60(8–9):1527–1529. https://doi.org/10.1016/S0022-3697(99)00165-1
Itoh H, Tse JS, Kawamura K (2001) The structure and dynamics of doubly occupied Ar hydrate. J Chem Phys 115:9414. https://doi.org/10.1063/1.1414378
Jeffrey GA (1969) Water structure in organic hydrates. Acc Chem Res 2(11):344–352. https://doi.org/10.1021/ar50023a004
Jeffrey GA (1984) Hydrate inclusion compounds. J Incl Phenom 1:211–222. https://doi.org/10.1007/BF00656757
Jeffrey GA, McMullan RK (1967) The clathrate hydrates. In: Cotton FA (eds) Book series: progress in inorganic chemistry, vol 8, pp 43–108. https://doi.org/10.1002/9780470166093.ch2
Kadobayashi H, Hirai H, Ohfuji H, Kojima Y, Ohishi Y, Hirao N, Ohtake M, Yamamoto Y (2017) Transition mechanism of sH to filled-ice Ih structure of methane hydrate under fixed pressure condition. J Phys Conf Ser 950:042044. https://doi.org/10.1088/1742-6596/950/4/042044
Kadobayashi H, Hirai H, Ohfuji H, Ohtake M, Yamamoto Y (2018) In situ Raman and X-ray diffraction studies on the high pressure and temperature stability of methane hydrate up to 55 GPa. J Chem Phys 148:1503. https://doi.org/10.1063/1.5013302
Kadobayashi H, Hirai H, Ohfuji H, Ohtake M, Muraoka M, Yoshida S, Yamamoto Y (2020a) Structural evolution of methane hydrate under pressures up to 134 GPa. J Chem Phys 152:194308. https://doi.org/10.1063/5.0007511
Kadobayashi H, Hirai H, Suzuki K, Ohfuji H, Muraoka M, Yoshida S, Yamamoto Y (2020b) Sequential in situ Raman spectroscopy for observing dissociation behavior of filled-ice Ih of methane hydrate at high pressure. J Raman Spectrosc 51:2536–2542. https://doi.org/10.1002/jrs.6012
Kadobayashi H, Hirai H, Ohfuji H, Kawamura H, Muraoka M, Yoshida S, Yamamoto Y (2020c) Effect of ammonia on mMethane hydrate stability under high-pressure and high-temperature conditions. J Phys Chem A 124:10890–10896. https://doi.org/10.1021/acs.jpca.0c09652
Kadobayashi H, Ohnishi S, Ohfuji H, Yamamoto Y, Muraoka M, Yoshida S, Hirao N, Kawaguchi-Imada S, Hirai H (2021) Diamond formation from methane hydrate under the internal conditions of giant icy planets. Sci Rep 11:8165. https://doi.org/10.1038/s41598-021-87638-5
Kamb B (1965) Aclathrate crystalline form of silica. Science 148:232–234. https://doi.org/10.1038/ncomms1196
Kawaji H, Horie H, Yamanaka S, Ishikawa M (1995) Superconductivity in the silicon clathrate compound (Na, Ba) xSi46. Phys Rev Lett 74:1427–1429. https://doi.org/10.1103/PhysRevLett.74.1427
Kieffer SW, Lu X, Bethke CM, Spencer JR, Marshak S, Navrotsky A (2006) A clathrate reservoir hypothesis for Enceladus' south polar plume. Science 314:1764. https://doi.org/10.1126/science.1133519
Kirchner MT, Boese R, Billups WE, Norman LR (2004) Gas hydrate single-crystal structure analyses. J Am Chem Soc 126:9407–9412. https://doi.org/10.1021/ja049247c
Kolesnikov A, Kutcherov VG, Goncharov AF (2009) Methane-derived hydrocarbons produced under upper-mantle conditions. Nat Geosci 2:566–570. https://doi.org/10.1038/ngeo591
Kraus D (2018) On Neptune, it's raining diamonds. Am Sci 106:285. https://doi.org/10.1511/2018.106.5.285
Kraus D, Vorberger J, Pak A, Hartley E, Gamboa EJ, Gericke DO, Glenzer SH, Granados E, MacDonald MJ, MacKinnon AJ, McBride EE, Nam I, Neumayer P, Roth M, Saunders AM, Schuster AK, Sun P, van Driel T, Döppner T, Falcone RW (2017) Formation of diamonds in laser-compressed hydrocarbons at planetary interior conditions. Nat Astron 1:606–611. https://doi.org/10.1038/s41550-017-0219-9
Kuhs WF, Chazallon B, Radaelli PG, Pauer F (1997) Cage occupancy and compressibility of deuterated N2-clathrate hydrate by neutron diffraction. J Incl Phenom Mol Recognit Chem 29:65–77. https://doi.org/10.1023/A:1007960217691
Kuhs WF, Hansen TC, Falenty A (2018) Filling ices with helium and the formation of helium clathrate hydrate. J Phys Chem Lett 9:3194–3198. https://doi.org/10.1021/acs.jpclett.8b01423
Kurnosov AV, Manakov AY, Komarov VY, Voronin VI, Teplykh AE, Dyadin YA (2001) A new gas hydrate structure. Dokl Phys Chem 381:303. https://doi.org/10.1023/A:1013293514290
Kvenvolden KA (1998) Methane hydrate—a major reservoir of carbon in the shallow geosphere? Chem Geol 71:41–51. https://doi.org/10.1016/0009-2541(88)90104-0
Lee MS, Scandolo S (2011) Mixtures of planetary ices at extreme conditions. Nat Commun 2:185. https://doi.org/10.1038/ncomms1184
Lee H, Lee J, Kim DY, Park J, Seo Y, Zeng H, Moudrakovski IL, Ratcliffe CI, Ripmeester JA (2005) Tuning clathrate hydrates for hydrogen storage. Nature 434:743–746. https://doi.org/10.1038/nature03457
Lei J, Lim J, Kim M, Yoo CS (2021) Crystal structure of symmetric ice X in H_2O–H_2 and H_2O–He under pressure. J Phys Chem Lett 12:4707–4712. https://doi.org/10.1021/acs.jpclett.1c00606
Li B, Ding Y, Kim DY, Wang L, Weng T-C, Yang W, Yu Z, Ji C, Wang J, Shu J, Chen JJ, Yang K, Xiao Y, Chow P, Shen G, Mao WL, Mao HK (2021) Probing the electronic band gap of solid hydrogen by inelastic X-ray scattering up to 90 GPa. Phys Rev Lett 126:036402. https://doi.org/10.1103/PhysRevLett.126.036402
Lin J, Gregoryanz E, Struzhkin V, Somayazulu M, Mao H, Hemley R (2005) Melting behavior of H2O at high pressures and temperatures. Geophys Res Lett 32:L11306. https://doi.org/10.1029/2005GL022499
Lobanov S, Chen P, Chen X, Zha C, Litasov K, Mao H, Goncharov A (2013) Carbon precipitation from heavy hydrocarbon fluid in deep planetary interiors. Nat Commun 4:2446. https://doi.org/10.1038/ncomms3446
Lokshin KA, Zhao Y, He D, Mao WL, Mao HK, Hemley RJ, Lobanov MV, Greenblatt M (2004) Structure and dynamics of hydrogen molecules in the novel clathrate hydrate by high pressure neutron diffraction. Phys Rev Lett 93:125503. https://doi.org/10.1103/PhysRevLett.93.125503
Londono D, Kuhs WF, Finney JL (1988) Enclathration of helium in ice II: the first helium hydrate. Nature 332:141–142. https://doi.org/10.1038/332141a0
Lorenzana HE, Silvera IF, Goettel KA (1989) Evidence for a structural phase transition in solid hydrogen at megabar pressures. Phys Rev Lett 63:2080. https://doi.org/10.1103/PhysRevLett.63.2080
Loveday JS, Nelmes RJ (2008) High-pressure gas hydrates. Phys Chem Chem Phys 10:937–950. https://doi.org/10.1039/B704740A
Loveday JS, Nelmes RJ, Guthrie M, Belmonte SA, Allan DR, Klug DD, Tse JS, Handa YP (2001a) Stable methane hydrate above 2 GPa and the source of Titan's atmosphericmethane. Nature 410:661–663. https://doi.org/10.1038/35070513
Loveday JS, Nelmes RJ, Guthrie M, Klug DD, Tse JS (2001b) Transition from cage clathrate to filled ice: the structure of methane hydrate III. Phys Rev Lett 87:215501. https://doi.org/10.1103/PhysRevLett.87.215501
Lunine JI, Stevenson DJ (1987) Clathrate and ammonia hydrates at high-pressure: application to the origin of methane on Titan. Icarus 70:61–77. https://doi.org/10.1016/0019-1035(87)90075-3
Machida S, Hirai H, Kawamura T, Yamamoto Y, Yagi T (2006) A new high-pressure structure of methane hydrate surviving to 86 GPa and its implications for the interiors of giant planets. Phys Earth Planet Inter 155:170–176. https://doi.org/10.1016/j.pepi.2005.12.008
Machida S, Hirai H, Kawamura T, Yamamoto Y, Yagi T (2007) Raman spectra of methane hydrate up to 86 GPa. Phys Chem Miner 34:31–35. https://doi.org/10.1007/s00269-006-0126-6
Machida S, Hirai H, Kawamura T, Yamamoto Y, Yagi T (2008) Structural changes of filled ice Ic structure for hydrogen hydrate under high pressure. J Chem Phys 129:224505. https://doi.org/10.1063/1.3013440
Machida S, Hirai H, Kawamura T, Yamamoto Y, Yagi T (2010) Raman spectra for hydrogen hydrate under high pressure: intermolecular interactions in filled icelc structure. J Phys Chem Solids 71:1324–1328. https://doi.org/10.1016/j.jpcs.2010.05.015

Magdău IB, Ackland GJ (2013) Identification of high-pressure phases III and IV in hydrogen: simulating Raman spectra using molecular dynamics. Phys Rev B 87:174110. https://doi.org/10.1103/PhysRevB.87.174110
Mak TCW, McMullan RK (1965) Polyhedral clathrate hydrates. X. Structure of the double hydrate of tetrahydrofuran and hydrogen sulfide. J Chem Phys 42:2732. https://doi.org/10.1063/1.1703229
Manakov AY, Dyadin YA, Ogienko AG, Kurnosov AV, Aladko EY, Larionov EG, Zhurko FV, Voronin VI, Berger IF, Goryainov SV, Lihacheva AY, Ancharov AI (2009) Phase diagram and high-pressure boundary of hydrate formation in the carbon dioxide-water system. J Phys Chem B 113:7257–7262. https://doi.org/10.1021/jp9008493
Mao H-K, Hemley RJ (1994) Ultrahigh-pressure transitions in solid hydrogen. Rev Mod Phys 66:671. https://doi.org/10.1103/RevModPhys.66.671
Mao WL, Mao H-K (2004) Hydrogen storage in molecular compounds. PNAS 101:708–710. https://doi.org/10.1073/pnas.0307449100
Mao WL, Mao HK, Goncharov AF, Struzhkin VV, Guo Q, Hu J, Shu J, Hemley RJ, Somayazulu M, Zhao Y (2002) Hydrogen clusters in clathrate hydrate. Science 297:2247–2249. https://doi.org/10.1126/science.1075394
Mao W, Koh CA, Sloan ED (2007) Clathrate hydrates under pressure. Phys Today 60:42. https://doi.org/10.1063/1.2800096
Marboeuf U, Mousis O, Petit JM, Schmitt B (2010) Clathrate hydrates formation in short-period comets. Astrophys J 708:812–816. https://doi.org/10.1088/0004-637X/708/1/812
Maynard-Casely HE, Lundegaard LF, Loa I, McMahon MI, Gregoryanz E, Nelmes RJ, Loveday JS (2014) The crystal structure of methane B at 8 GPa—an α-Mn arrangement of molecules. J Chem Phys 141:234313. https://doi.org/10.1063/1.4903813
Mazin II, Hemley RJ, Goncharov AF, Hanfland M, Mao HK (1997) Quantum and classical orientational ordering in solid hydrogen. Phys Rev Lett 78:1066. https://doi.org/10.1103/PhysRevLett.78.1066
McMullan RK, Jeffrey GA (1965) Polyhedral clathrate hydrates. IX. Structure of ethylene oxide hydrate. J Chem Phys 42:2725. https://doi.org/10.1063/1.1703228
Morales MA, Pierleoni C, Schwegler E, Ceperley DM (2010) Evidence for a first order liquid–liquid transition in high pressure hydrogen from ab-initio simulations. PNAS 107(29):12799–12803. https://doi.org/10.1073/pnas.1007309107
Nakagawa T, Kihara K, Harada K (2001) The crystal structure of low melanophlogite. Am Miner 86:1506–1512. https://doi.org/10.2138/am-2001-11-1219
Nakahata I, Matsui N, Akahama Y, Kawamura H (1999) Structural studies of solid methane at high pressures. Chem Phys Lett 302(3–4):359–362
Nakano S, Moritoki M, Ohgaki K (1998) High-pressure phase equilibrium and Raman microprobe spectroscopic studies on the CO_2 hydrate system. J Chem Eng Data 43:807–810. https://doi.org/10.1021/je9800555
Naumova AS, Lepeshkin SV, Bushlanov PV, Oganov AR (2021) Unusual chemistry of the C–H–N–O system under pressure and implications for giant planets. J Phys Chem A 125:3936–3942. https://doi.org/10.1021/acs.jpca.1c00591
Nettelmann N, Helled R, Fortney JJ, Redmer R (2013) New indication for a dichotomy in the interior structure of Uranus and Neptune from the application of modified shape and rotation data. Planet Space Sci 77:143–151. https://doi.org/10.1016/j.pss.2012.06.019
Nettelmann N, Wang K, Fortney JJ, Hamel S, Yellamilli S, Bethkenhagen M, Redmer R (2016) Uranus evolution models with simple thermal boundary layers. Icarus 275:107–116. https://doi.org/10.1016/j.icarus.2016.04.008
Nolas GS, Slack GA, Morelli DT, Tritt TM, Ehrlich AC (1996) The effect of rare-earth filling on the lattice thermal conductivity of skutterudites. J Appl Phys 79:4002–4008. https://doi.org/10.1063/1.361828
Ohgaki K, Akano K, Sangawa H, Matsubara T, Nakano S (1996) Methane exploitation by carbon dioxide from gas hydrates-phase equilibria for CO_2–CH_4 mixed hydrate system. J Chem Eng 29:478–483. https://doi.org/10.1252/jcej.29.478
Ohta K, Ichimaru K, Einaga M, Kawaguchi S, Shimizu K, Matsuoka T, Hirao N, Ohishi Y (2015) Phase boundary of hot dense fluid hydrogen. Sci Rep 5:16560. https://doi.org/10.1038/srep16560
Okuchi T, Takigawa M, Shu J, Mao H, Hemley R, Yagi T (2007) Fast molecular transport in hydrogen hydrates by high-pressure diamond anvil cell NMR. Pys Rev B 75:144104. https://doi.org/10.1103/PhysRevB.75.144104
Pellenbarg RE, Max MD, Stephen M, Clifford SM (2003) Methane and carbon dioxide hydrates on Mars: potential origins, distribution, detection, and implications for future in situ resource utilization. J Geophys Res 108:8042. https://doi.org/10.1029/2002JE001901
Petrenko VF, Whitworth RW (1999) Physics of ice. Oxford University Press, New York, pp 4, 6, 252 ISBN:0-19-851895-1
Pratt LR, Chandler D (1977) Theory of the hydrophobic effect. J Chem Phys 67:3683. https://doi.org/10.1063/1.435308
Pruzan P (1994) Pressure effects on the hydrogen bond in ice up to 80 GPa. J Mol Struct 322:279–286. https://doi.org/10.1016/0022-2860(94)87045-4
Qian GR, Lyakhov AO, Zhu Q, Oganov AR, Dong X (2014) Novel hydrogen hydrate structures under pressure. Sci Rep 4:5606. https://doi.org/10.1038/srep05606
Redmer R, Mattsson TR, Nettelmann N, French M (2011) The phase diagram of water and the magnetic fields of Uranus and Neptune. Icarus 211:798–803. https://doi.org/10.1016/j.icarus.2010.08.008
Ripmeester JA, Ratcliffe CI (1999) On the contributions of NMR spectroscopy to clathrate science. J Struct Chem 40:654–662. https://doi.org/10.1063/1.3124187
Ripmeester JA, Garg SK, Davidson DW (1980) NMR behavior of the clathrate hydrate of tetrahydrofuran. III. Effect of oxygen. J Magn Reson 38:537–544. https://doi.org/10.1016/0022-2364(80)90333-9
Ripmeester JA, Tse JS, Ratcliffe CI, Powell BM (1987) A new clathrate hydrate structure. Nature 325:135–136. https://doi.org/10.1038/325135a0
Ripmeester JA, Ratcliffe CI, Klug DD, Tse JS (1994) Molecular perspectives on structure and dynamics in clathrate hydrates. Annuals of the New York Academy of Sciences, 715:161–176. In: Sloan ED, Happel J, Hnatow MA (eds) Proc. First International Conference on Natural Gas Hydrates. https://doi.org/10.1111/j.1749-6632.1994.tb38832.x
Ross M (1981) The ice layer in Uranus and Neptune—diamonds in the sky? Nature 292:435–436. https://doi.org/10.1038/292435a0
Saito S (1994) Materials with fullerene-related structures. Rev High Press Sci Technol 3–2:150–155 (**in Japanese with English abstract**)
Salzmann CG, Radaelli PG, Hallbrucker A, Mayer E, Finney JL (2009a) The preparation and structures of hydrogen ordered phases of ice. Science 311:1761–1758. https://doi.org/10.1126/science.1123896
Salzmann CG, Radaelli PG, Mayer E, Finney JL (2009b) Ice XV. A new thermodynamically stable phase of ice. Phys Rev Lett 103:105701. https://doi.org/10.1103/PhysRevLett.103.105701
Sandford S, Allamandola L, Geballe T (1993) Spectroscopic detection of molecular hydrogen frozen in interstellar ices. Science 262:400. https://doi.org/10.1126/science.11542874
Sakai H, Gamo T, Kim ES, Tsutsumi M, Tanaka T, Ishibashi J, Wakita H, Yamano M, Oomori T (1990) Venting of carbon dioxide-rich fluid and hydrate formation in mid-Okinawa trough backarc basin. Science 248(4959):1093–1096. https://doi.org/10.1126/science.248.4959.1093
Sasaki S, Kito Y, Kume T, Shimizu H (2007) High-pressure Raman study on the guest vibration in the host cage of methane hydrate structure I. Chem Phys Lett 444:91. https://doi.org/10.1016/j.cplett.2007.07.018
Schaack S, Ranieri U, Depondt P, Gaal R, Kuhs WF, Falenty A, Gillet P, Finocchi F, Bove LE (2018) Orientational ordering, locking-in, and distortion of CH4 molecules in methane hydrate III under high pressure. J Phys Chem C 122:11159–11166. https://doi.org/10.1021/acs.jpcc.8b02783
Schaack S, Ranieri U, Depondt P, Gaal R, Kuhs WF, Gillet P, Finocchi F, Bove LE (2019) Observation of methane filled hexagonal ice stable up to 150 GPa. PNAS 116:16204–16209. https://doi.org/10.1073/pnas.1904911116
Schaack S, Depondt P, Moog M, Pietrucci F, Finocchi F (2020) How methane hydrate recovers at very high pressure the hexagonal ice structure. J Chem Phys 152:024504. https://doi.org/10.1063/1.5129617
Schicks JM, Naumann R, Erzinger J, Hester KC, Koh CA, Sloan ED (2006) Phase transitions in mixed gas hydrates: experimental observations versus calculated data. J Phys Chem B 110:11468–11474. https://doi.org/10.1021/jp0612580
Senadheera L, Conradi MS (2007) Rotation and diffusion of H2 in hydrogen-ice clathrate by 1H NMR. J Phys Chem B 111:12097–12102. https://doi.org/10.1021/jp074517+
Shimizu H, Kumazaki T, Kume T, Sasaki S (2002) In situ observations of high-pressure phase transformations in a synthetic methane hydrate. J Phys Chem B 106:30–33. https://doi.org/10.1021/jp013010a

Silvera IF, Dias R (2022) Phases of the hydrogen isotopes under pressure: metallic hydrogen. Adv Phys X 6:1961607. https://doi.org/10.1080/23746149.2021.1961607
Sloan ED (2007) Physical/chemical properties of gas hydrates and application to world margin stability and climatic change. Geol Soc Lond Spec Publ 137:31–50. https://doi.org/10.1144/GSL.SP.1998.137.01.03
Sloan ED, Koh CA (2008) Clathrate hydrates of natural gases, 3rd edn. Taylor and Francis, London, pp 45, 257, 320, and 537. ISBN-13: 978-0849390784
Strobel TA, Sloan ED, Koh CA (2009) Raman spectroscopic studies of hydrogen clathrate hydrates. J Chem Phys 130:014506. https://doi.org/10.1063/1.3046678
Strobel TA, Somayazulu M, Hemley RJ (2011) Phase behavior of $H_2 + H_2O$ at high pressures and low temperatures. J Phys Chem C 115:4898–4903. https://doi.org/10.1063/1.3046678
Strobel TA, Somayazulu M, Sinogeikin SV, Dera P, Hemley RJ (2016) Hydrogen-stuffed, quartz-like water ice. J Am Chem Soc 138:13786–13789. https://doi.org/10.1021/jacs.6b06986
Struzhkin VV, Militzer B, Mao WL, Mao H-K, Hemley R (2007) Hydrogen storage in molecular clathrates. Chem Rev 107:4133–4151. https://doi.org/10.1021/cr050183d
Sugimura E, Iitaka T, Hirose K, Kawamura K, Sata N, Ohishi Y (2008) Compressionof H2Oice to 126 GPa and implications for hydrogen-bondsymmetrization: synchrotron x-ray diffraction measurements anddensity-functional calculations. Phys Rev B 77:2103. https://doi.org/10.1103/PhysRevB.77.214103
Takeya S, Udachin KA, Moudrakovski IL, Susilo R, Ripmeester JA (2010) Direct space methods for powder X-ray diffraction for guest-host materials: applications to cage occupancies and guest distributions in clathrate hydrates. J Am Chem Soc 132:524–531. https://doi.org/10.1021/ja905426e
Tanaka T, Hirai H, Matsuoka T, Ohishi Y, Yagi T, Ohtake M, Yamamoto Y, Nakano S, Irifune T (2013) Phase changes of filled ice Ih methane hydrate under low temperature and high pressure. J Chem Phys 139:104701. https://doi.org/10.1063/1.4820358
Tobie G, Grasset O, Lunine JI, Mocquet A, Sotin C (2005) Titan's internal structure inferred from a coupled thermal-orbital model. Icarus 175:496–502. https://doi.org/10.1016/j.icarus.2004.12.007
Toledano P, Katzke H, Goncharov AF, Hemley RJ (2009) Symmetry breaking in dense hydrogen: mechanisms for the transitions to phase II and phase III. Phys Rev Lett 103:105301-1–105304. https://doi.org/10.1103/PhysRevLett.103.105301
Tulk C, Klug D, Santos A, Karotis G, Guthrie M, Molaison J, Pradhan N (2012) Cage occupancies in the high pressure structure H methane hydrate: a neutron diffraction study. J Chem Phys 136:054502. https://doi.org/10.1063/1.3679875
Tulk CA, Machida S, Klug DD, Lu H, Guthrie M, Molaison JJ (2014) The structure of CO_2 hydrate between 0.7 and 1.0 GPa. J Chem Phys 141:1503. https://doi.org/10.1063/1.4899265
Udachin KA, Ratcliffe CI, Enright GD, Ripmeester JA (1997) Structure H hydrate: a single crystal diffraction study of 2,2-dimethylpentane·5(Xe, H2S)·34H2O. Supramol Chem 8:173–176. https://doi.org/10.1080/10610279708034933
Udachin KA, Ratcliffe CI, Ripmeester JA (2002) Single crystal diffraction studies of structure I, II and H hydrates: structure, cage occupancy and composition. J Supramol Chem 2:405–408. https://doi.org/10.1016/S1472-7862(03)00049-2
Umemoto S, Yoshii T, Akahama Y, Kawamura H (2002) X-ray diffraction measurements for solid methane at high pressures. J Phys Condens Matter 14(44):10675–10678. https://doi.org/10.1088/0953-8984/14/44/355
Vos WL, Finger LW, Hemley RJ, Mao HK (1993) Novel H_2–H_2O clathrates at high pressures. Phys Rev Lett 71:3150. https://doi.org/10.1103/PhysRevLett.71.3150
Vos WL, Finger LW, Hemley RJ, Mao HK (1996) Pressure dependence of hydrogen bonding in a novel H_2O–H_2 clathrate. Chem Phys Lett 257:524. https://doi.org/10.1016/0009-2614(96)00583-0
Wang Y, Glazyrin K, Roizen V, Oganov AR, Chernyshov I, Zhang X, Greenberg E, Prakapenka VB, Yang X, Jiang SQ, Goncharov AF (2020) Novel hydrogen clathrate hydrate. Phys Rev Lett 125:255702. https://doi.org/10.1103/PhysRevLett.125.255702
Wentorf RH (1965) The behavior of some carbonaceous materials at very high pressures and high temperatures. J Phys Chem 69:3063–3069. https://doi.org/10.1021/j100893a041
Wigner E, Huntington HB (1935) On the possibility of a metallic modification of hydrogen. J Chem Phys 3:764. https://doi.org/10.1063/1.1749590
Yagi T, Iida E, Hirai H, NMiyajima N, Kikegawa T, Bunno M, (2007) High-pressure behavior of a SiO_2 clathrate observed by using various pressure media. Phys Rev B 75:174115. https://doi.org/10.1103/PhysRevB.75.174115
Zerr A, Serghiou G, Boehler R, Ross M (2006) Decomposition of alkanes at high pressures and temperatures. High Press Res 26:23–32. https://doi.org/10.1080/08957950600608931
Zha CS, Liu Z, Hemley RJ (2012) Synchrotron infrared measurements of dense hydrogen to 360 GPa. Phys Rev Lett 108:146402. https://doi.org/10.1103/PhysRevLett.108.146402
Zhang J, Kuon J-L, Iitaka T (2012) First principles molecular dynamics study of filled ice hydrogen hydrate. J Chem Phys 137:084505. https://doi.org/10.1063/1.4746776
Zhang X, Wang Y, Bykov M, Bykova E, Chariton S, Prakapenka VB, Glazyrin K, Goncharov AF (2021) Immiscibility in N_2–H_2O solids up to 140 GPa. J Chem Phys 154:2505. https://doi.org/10.1063/5.0052315
Zhao Z, Shen B, Zhu JM, Lang X, Wu G, Tan D, Pei H, Huang T, Ning M, Ma H (2021) Active methanogenesis during the melting of Marinoan snowball Earth. Nat Commun 12:955. https://doi.org/10.1038/s41467-021-21114-6

Publisher's Note